AD

TECHNICAL REPORT ECOM - 01412 - F

RADIATION EFFECTS ON DIELECTRIC MATERIALS

FINAL REPORT

By

J. F. COLWELL, D. W. De MICHELE, AND R. F. OVERMYER

DECEMBER 1966

THIS RESEARCH WAS SPONSORED BY THE DEFENSE ATOMIC SUPPORT AGENCY UNDER NWER SUBTASK NO. 16.0091

ECOM

UNITED STATES ARMY ELECTRONICS COMMAND · FORT MONMOUTH, N.J.
CONTRACT DA28-043 AMC-01412(E)

GENERAL DYNAMICS
General Atomic Division
SPECIAL NUCLEAR EFFECTS LABORATORY
SAN DIEGO, CALIFORNIA

Technical Report ECOM-01412-F
GA-7474

RCS OSD-1366
December 1966

RADIATION EFFECTS ON DIELECTRIC MATERIALS

FINAL REPORT

1 July 1966 through 30 September 1966

Report No. 5

CONTRACT DA28-043 AMC-01412(E)
AMC Code 5900.21.830.44.00

Prepared by
J. F. Colwell, D. W. DeMichele, and R. F. Overmyer
General Atomic Division, General Dynamics Corporation
Special Nuclear Effects Laboratory
San Diego, California

For

U. S. Army Electronics Command, Fort Monmouth, N. J.

This research was sponsored by the Defense Atomic Support Agency under NWER Subtask Number 16.0091.

ABSTRACT

A detailed description of the techniques and equipment employed in the ion-implantation process is presented. Results of high-energy electron irradiation of a Mylar capacitor with ion-implanted electrodes are compared to the response of a control sample. The ion-implanted electrodes exhibit better carrier injection than conventional foil electrodes. Transient radiation effects data from irradiation of a monolithic ceramic capacitor and two glass capacitors are included. One of the glass capacitors contained a semicrystalline dielectric with very high dielectric constant. The transient radiation effects in Mylar versus temperature appear to fit a band model for the conduction process in which a continuous distribution of carrier traps is located in the forbidden zone and one sign of carrier is immobilized. An examination of the energy loss processes of moderately fast electrons in insulators indicates that from 15 eV to 3 eV the energy loss is primarily to excitons whereas energy loss to optical and acoustical phonons occurs down to thermal energies.

FOREWORD

The objectives of this program were to determine the effects of gamma and neutron irradiation on dielectric materials and electronic parts and to apply this knowledge to the accurate prediction of radiation response in such parts. Further, models of electronic parts were to be developed which exhibit high radiation resistance.

This research was sponsored by the Defense Atomic Support Agency under NWer Subtask No. 16.0091 and was authorized by the Electronic Components Laboratory, U. S. Army Electronics Command, Fort Monmouth, N. J., under Contract DA 28-043AMC-01412(E), AMC Code 5900.21.830.44.00.

CONTENTS

Figures

1. INTRODUCTION

During the final quarter of the contract, the ion-implantation process of applying electrodes to Mylar film was perfected. In this process, metallic ions are accelerated into the substrate material to form a diffuse interface between the two materials while the surface is continually being cleaned by sputtering with an inert gas. Contacts on metals, semiconductors, and insulators have demonstrated strong physical bonding, good electrical contact, and low impurity concentration. A detailed description of the process and the equipment developed for ion implantation is included in this report. Results of linear accelerator (Linac) irradiation of a Mylar capacitor with ion-implanted electrodes are compared with a control sample which had foil electrodes. Although no dramatic differences were observed in the transient response, the signals did show dissimilarities, which are explainable on the basis of better carrier injection by the ion-implanted electrodes.

Irradiations were also performed with the Linac on a monolithic type of ceramic capacitor and on two types of glass capacitors. One of the glass capacitors had conventional glass dielectric, whereas the other was constructed with a new dielectric material, Glass-K, that has a high dielectric constant comparable to the barium titanate ceramic formulations. The difference in properties evident in Glass-K are due to the heat treatment given the dielectric material to change it from an amorphous glass to one which contains microcrystals.

Theoretical examination of the energy loss of relatively low energy electrons in insulators is presented to strengthen the arguments used in the theory of transient electrical effects in irradiated insulators.[1]

Further consideration of the results of the transient effects measurements in Mylar versus temperature that were discussed in the last quarterly report[2] are also included in this report.

Accelerator Pulsed Fast Assembly (APRA) irradiations were not performed during this quarterly period as the joint construction-operating permit had not yet been issued by the Atomic Energy Commission and the facility could not be completed.

2. TRANSIENT RADIATION EFFECTS IN A MYLAR CAPACITOR WITH ION-IMPLANTED ELECTRODES

A parallel-plate capacitor with ion-implanted aluminum electrodes on Mylar was constructed and irradiated with the Linac. The ion implantation process used to apply the aluminum electrodes on the 1-mil Type C Mylar is described in detail in Section 3. During each implantation, six 1 in. by 1 in. capacitor sections were processed on one side by masking such that an 0.8 in. by 0.8 in. electrode was implanted on each section. Twenty-four such sections were assembled with 1-mil lead foil interleaved in alternate directions between sections to provide the electrical contact to the implanted electrodes. Stiff fiberglass sheets held the capacitor sections together by means of metal clips at each end of the capacitor. The metal clips also provided electrical contacts to the lead foils brought out to each end. The construction was similar to that used in commercial silvered-mica capacitors. As the experiment was performed in vacuum to eliminate effects due to air ionization, no potting material was used to seal the capacitor except the epoxy used to keep the metal clips in place. A similar capacitor was constructed in the same manner using Mylar from the same original spool of film, but without the ion-implanted electrodes, for the control sample. Previous results of transient effects measurements of Mylar capacitors with foil electrode construction and metallized or vapor-plated Mylar had shown essentially no difference between the response of the two types.[3]

The two capacitors were irradiated with 30-MeV electrons from the Linac at 2×10^9 rads (Cu)/sec with 4-μsec pulses. The test circuit, utilizing a 10-kΩ series-measuring resistor, was described in an earlier report.[4] The results of the test were as follows:

1. The total signal (prompt plus delayed) was the same within a few percent in both types for the first pulse.

2. The total signal from the foil type for the tenth pulse was 5 to 10 percent less than the signal from the ion-implanted Mylar capacitor. The foil type achieved its final value after three to four pulses, or about 30,000 rads (Cu), whereas the signals from the ion-implanted capacitor decreased more slowly for eight to nine pulses, or about 90,000 rads (Cu). Figure 2.1 illustrates the magnitude of the response of the first and tenth pulses for each capacitor.

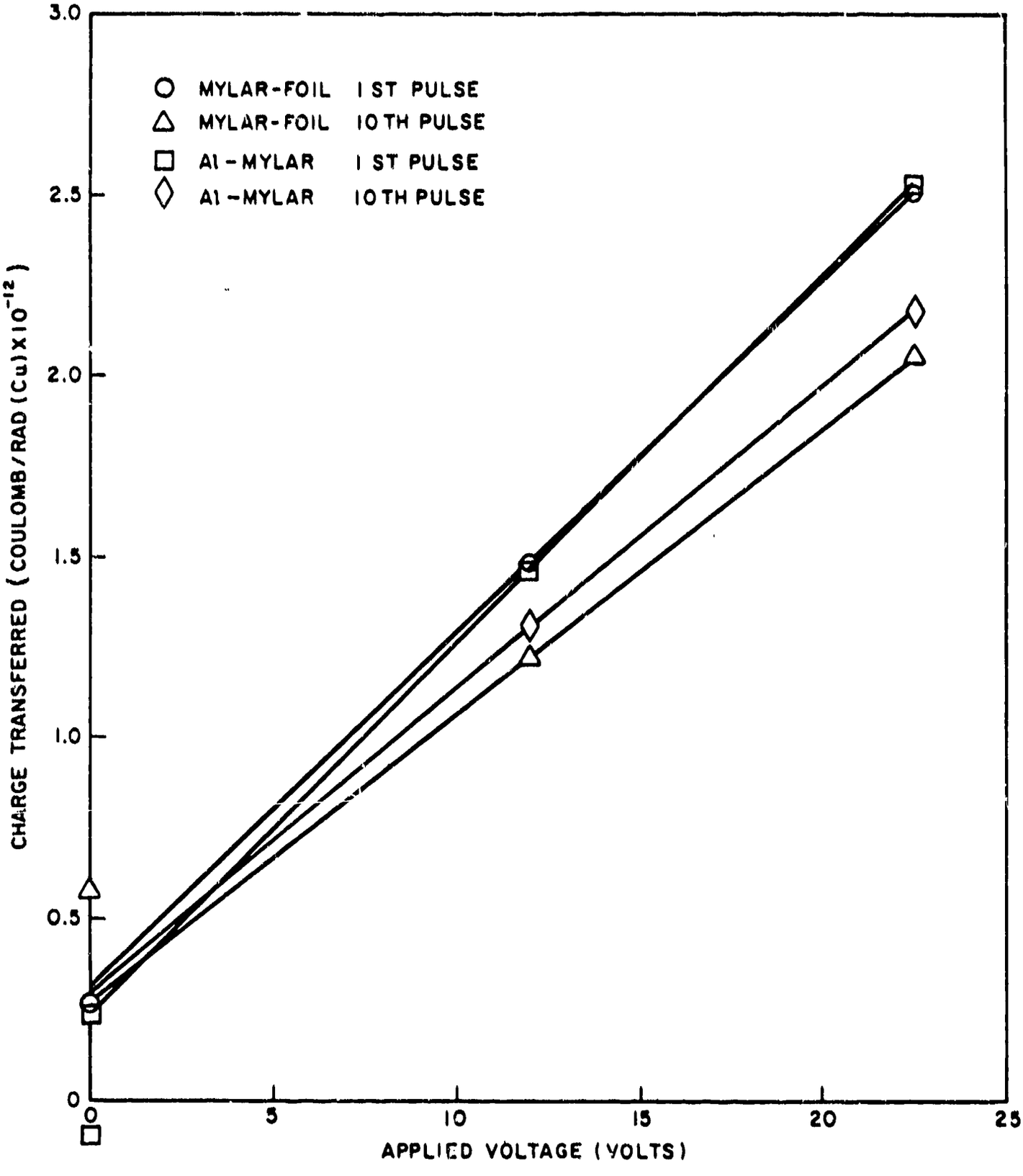

Fig. 2. 1--Total transient signal for two Mylar capacitors

3. The prompt signal was a few percent larger in the foil-type capacitor after correction for the different secondary emission signals at 0 V, as indicated in Fig. 2. 2.

4. The delayed component of conductivity was about 50 percent larger in the capacitor with the ion-implanted contacts. The tracings of the transient signals from both capacitors in Fig. 2. 3 show the difference in the delayed components after the initial prompt rise in the signal.

The observation that the transient-response signals decreased more slowly with succeeding pulses in the capacitor with the ion-implanted electrodes indicated that polarization was still taking place and that the electrodes were not perfectly injecting but that they were better than the foil type. During the pulse of ionizing radiation, the insulator-electrode interface is essentially bathed in a plasma such that there should have been little or no difference in the prompt response of the two capacitors. Slight material differences due to variations in the treatment of the two Mylar samples, such as the heating during the cleaning and implantation process, could account for the difference observed. The larger delayed conductivity signal in the ion-implanted type is an indication of a better electrode than the foil type, since the former allowed delayed charge to reach the contacts after the ionizing pulse and be observed in the external circuit rather than be trapped at the insulator-electrode interface.

Further investigations of the effects of varying the dose and dose rate are planned.

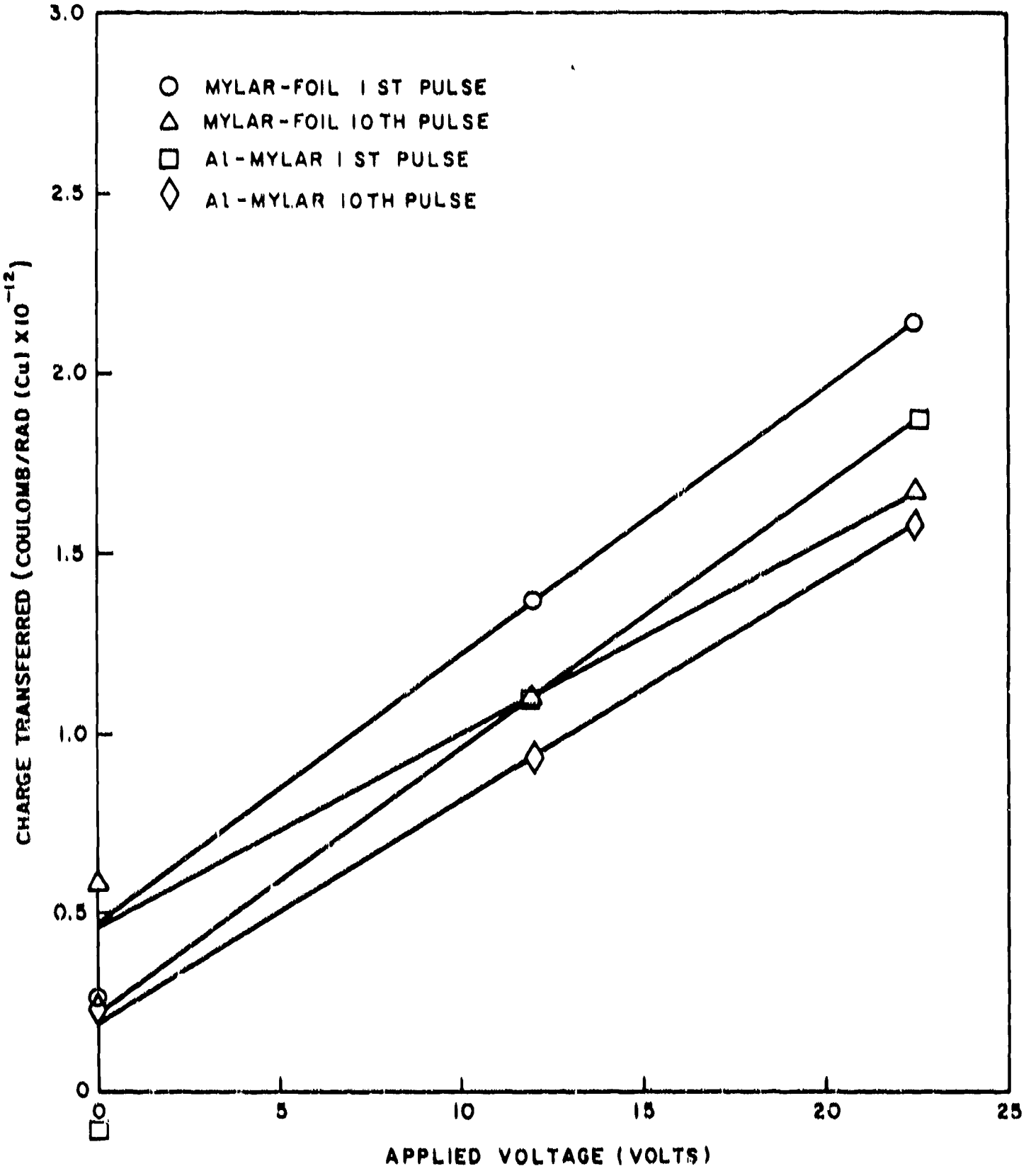

Fig. 2.2--Prompt signal from two Mylar capacitors

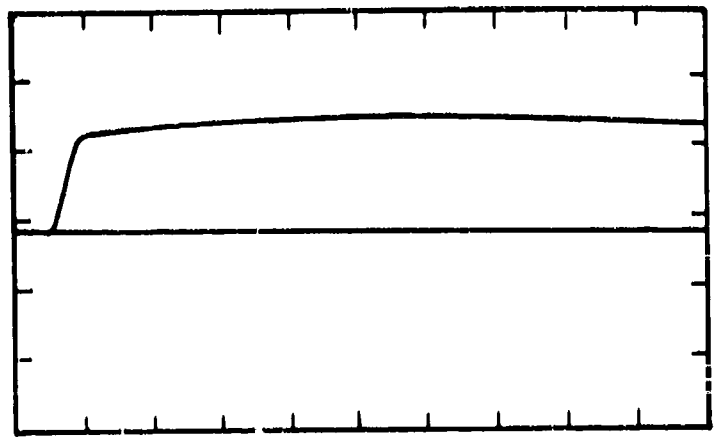

VERTICAL: 2 V/DIV

SWEEP: 10 μSEC/DIV

MYLAR-FOIL CAPACITOR RESPONSE,
11,700 RADS (Cu)

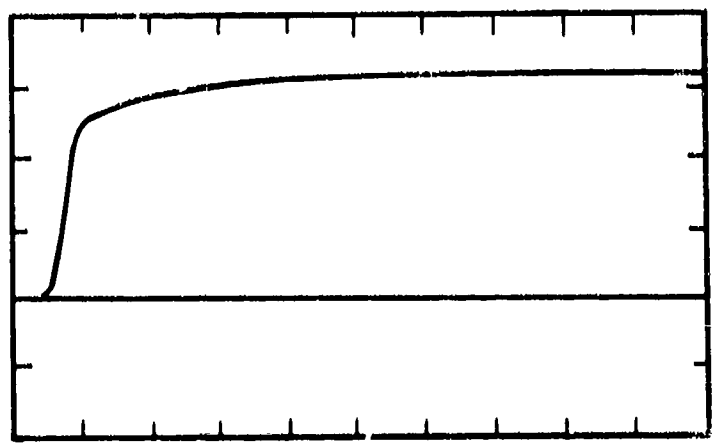

VERTICAL: 1 V/DIV

SWEEP: 10 μSEC/DIV

ION-IMPLANTED MYLAR CAPACITOR
RESPONSE, 14,400 RADS (Cu)

Fig. 2.3--Response of Mylar capacitors with +22.5 volts applied

3. ION-IMPLANTATION TECHNIQUE

3. 1. INTRODUCTION

A description of the techniques of ion implantation and the equipment utilized is given in this section. The techniques and the necessary support equipment have been developed in the past six months. The advantages and limitations of ion implantation are also pointed out.

Ion implantation, or ion plating, is used to form a diffused metallic interface between two dissimilar materials. The diffused surface layer provides a strong physical bond, good electrical contact, and low impurity concentrations. Insulators, semiconductors, and metals have been plated by this method, and each of these three different types of substrates requires a different approach to successfully implant a metal layer. Four articles by D. M. Mattox[5-8] were most helpful in developing the techniques which are described here.

3. 2. ION IMPLANTATION

In general, ion implantation consists in injecting metal ions into a substrate material. The metal ions are normally formed from a metal vapor in an argon plasma and the ions are accelerated toward the substrate by a large negative potential gradient. Upon arrival at the surface, the high-energy ions cause several interactions: they knock off physically adsorbed impurities; their high energy allows them to break the chemical bonds of oxides; and, finally, their momentum carries them deep into the lattice of the substrate. Some substrate atoms are displaced and sputtered into the vacuum, others form interstitials in the lattice. After a period of time, the surface of the substrate is free of chemically and physically adsorbed impurities and a diffused interface of the substrate and metal begins to form. As more and more metal ions are implanted, the surface becomes more metallic.

Metal ions have been formed by two different methods. The first method is to establish a plasma with a noble gas. The metal to be implanted is evaporated into the plasma, where it is ionized. These metal ions drift through the plasma and eventually fall through the potential gradient between the plasma and the cathode on which the substrate is mounted. The ions from this type of source are not monoenergetic. Most of these ions are, in fact, at low energies. This type of source is easier

to run and the equipment requirements are not as extensive as the second type of source. The second method of producing metal ions does not require a noble-gas partial pressure and the ions are essentially monoenergetic. The ions are formed inside a small chamber and extracted. These ions then fall through the full cathode potential.

The plasma implantation technique is illustrated schematically in Fig. 3. 1. Both methods will be discussed in more detail.

3. 3. THE VACUUM SYSTEM

A high-vacuum evaporator system is used to house the implanting equipment. This system has a clean base pressure of 7×10^{-7} torr. The system is composed of a fore pump, a molecular-sieve cryogenic trap on the fore line, a 4-in. oil diffusion pump, a cryogenically cooled chevron baffle, and an 18-in. Pyrex jar.

The stainless-steel base plate is equipped with various ports and feedthroughs. A linear rotary-motion feedthrough is available. Paddles attached to this feedthrough are used to baffle the pumping port when a slower pumping speed is desired and to optically shield a substrate from a metal-vapor source. An electrically insulated tube is located in the center of the vacuum system to leak in gas at a controlled rate. There are three different valves for controlling the leak rate into the system -- a variable leak valve is used for a fine control of the leak rate; a manual on-off valve is provided for manual control; and a solenoid valve, which is normally used in conjunction with the plasma-ion source, is located in series with the other two valves. The solenoid valve is operated by a meter relay. The meter relay monitors the current being drawn at the cathode. If the current exceeds a predetermined value, the solenoid is closed and the pressure in the vacuum system falls. With a decrease in pressure, the current also decreases. At a predetermined lower limit, the solenoid is opened and the pressure and current begin to rise slowly. Normally, the maximum current is set at 45 mA and the minimum current at 40 mA. The regulator can easily maintain the current within these limits. The prescribed operation of this leak-rate control system is as follows. The maximum and minimum values of the current is set on the meter relay; the manual and variable leak valves are closed. The cathode voltage is set at the prescribed voltage; the relay control switch is turned on. With the variable leak valve closed, the manual valve is opened; while the current meter on the power supply is monitored, the variable leak valve is slowly opened. The leak valve is adjusted until, with the solenoid in an open position, the current rises at a very slow rate. After the controls have been set in this way, the current will slowly oscillate between the two values set on the master relay.

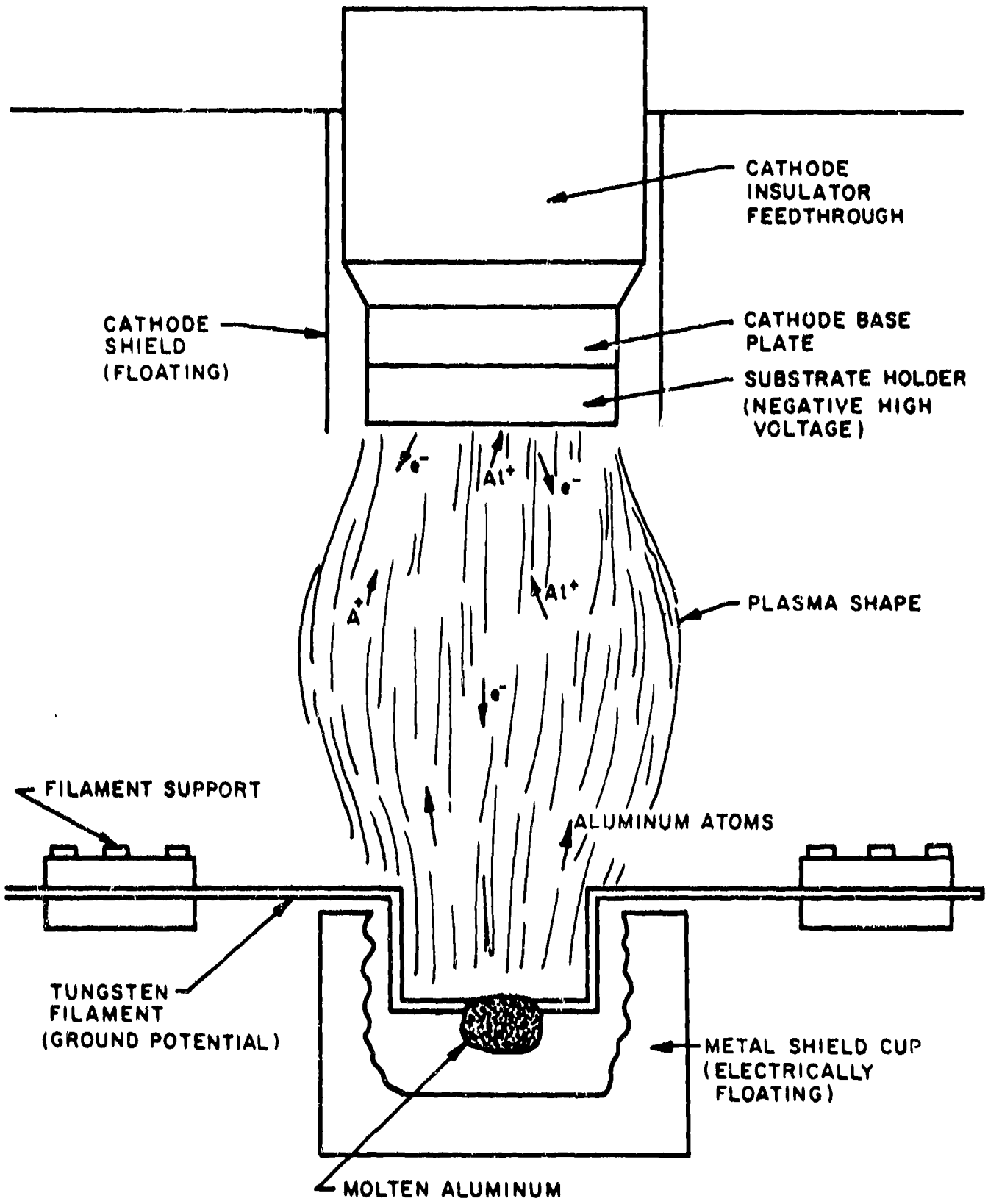

Fig. 3.1--Plasma implantation

There are two bell jars for this system. The first--a standard 18-in.-diam jar with a dome top--was used with the first series of tests. The substrate holder used with this jar had no facilities for heating or cooling the sample. The second jar is an 18-in.-diam, 24-in.-high cylinder, on top of which is a 19-in.-diam stainless steel flange. Six high-voltage feedthroughs are mounted on the flange. The sample holder used with this jar can be heated or cooled and the temperature of the sample mount can be monitored during the implantation.

3.4. SUPPORT EQUIPMENT

The high-voltage cathode power supply is normally run with a negative voltage output. Its output is with respect to ground. An interlock is provided such that when the bell jar is in an open position, the high voltage is interrupted. This supply is not well regulated, and the voltage changes with a changing current. It has a maximum voltage of 20,000 V and maximum current of 50 mA. The output lead of this supply is in series with a 50,000-ohm resistor, which acts as a partial current-limiting device and also stabilizes the discharge. A schematic of this support system is shown in Fig. 3.2.

3.5. CATHODE AND SHIELD DESIGN

In order to establish a localized plasma discharge, the cathode assembly and sample holder must be carefully designed as it is desirable to have the plasma strike only the face of the substrate holder. If the plasma strikes extraneous parts of the cathode, contaminants will be sputtered into the plasma, where they will be ionized and possibly implanted in the substrate. To localize the plasma to the area around the substrate holder, electrostatic shields are used. These shields also prevent the evaporated metal and ionized metal from coating the insulator that supports the cathode. As pointed out by Mattox,[5-8] these shields are effective only if they are placed within an electron mean free path of the cathode section to be shielded. A separation of 0.25 in. is quite effective for pressures less than 20μ. If it is desired to have the argon pressure higher than that, the separation distance must be reduced. Electrically, the shields are allowed to float. The cathode, of course, is at a high negative potential with respect to ground. Two different cathode shield designs have worked quite well. The first cathode design, as previously mentioned, has no provisions for temperature control or temperature monitoring. A nondimensional drawing of this shield design is shown in Fig. 3.3. The second cathode assembly, which is now being used, has these provisions. Schematics for the isolation transformers, heaters, and thermocouples are given in Figs. 3.2 and 3.4. A scale drawing for the second cathode design is given in Fig. 3.5. All temperature control and monitoring can be done while the cathode assembly is at high voltage.

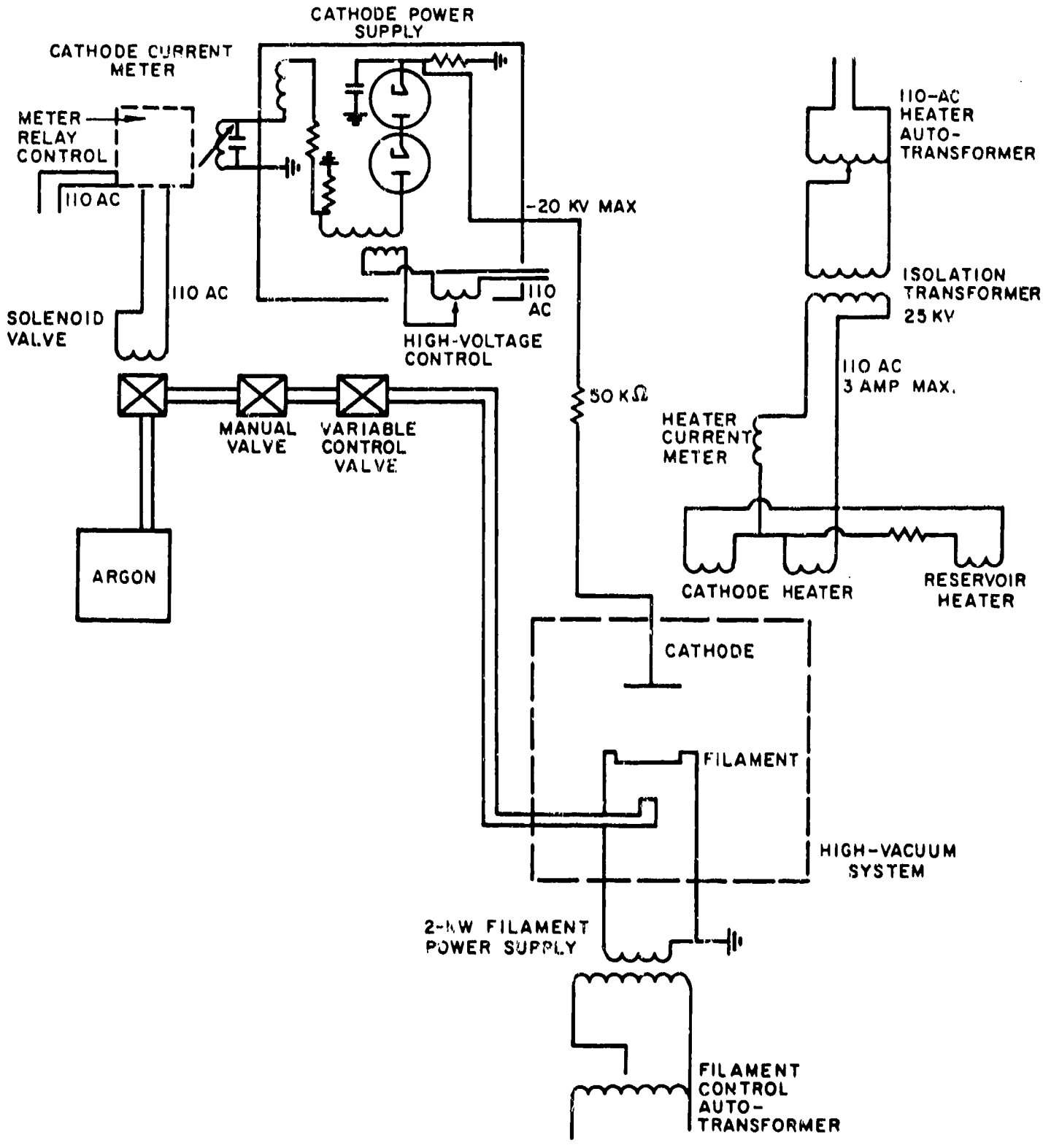

Fig. 3.2--Support equipment

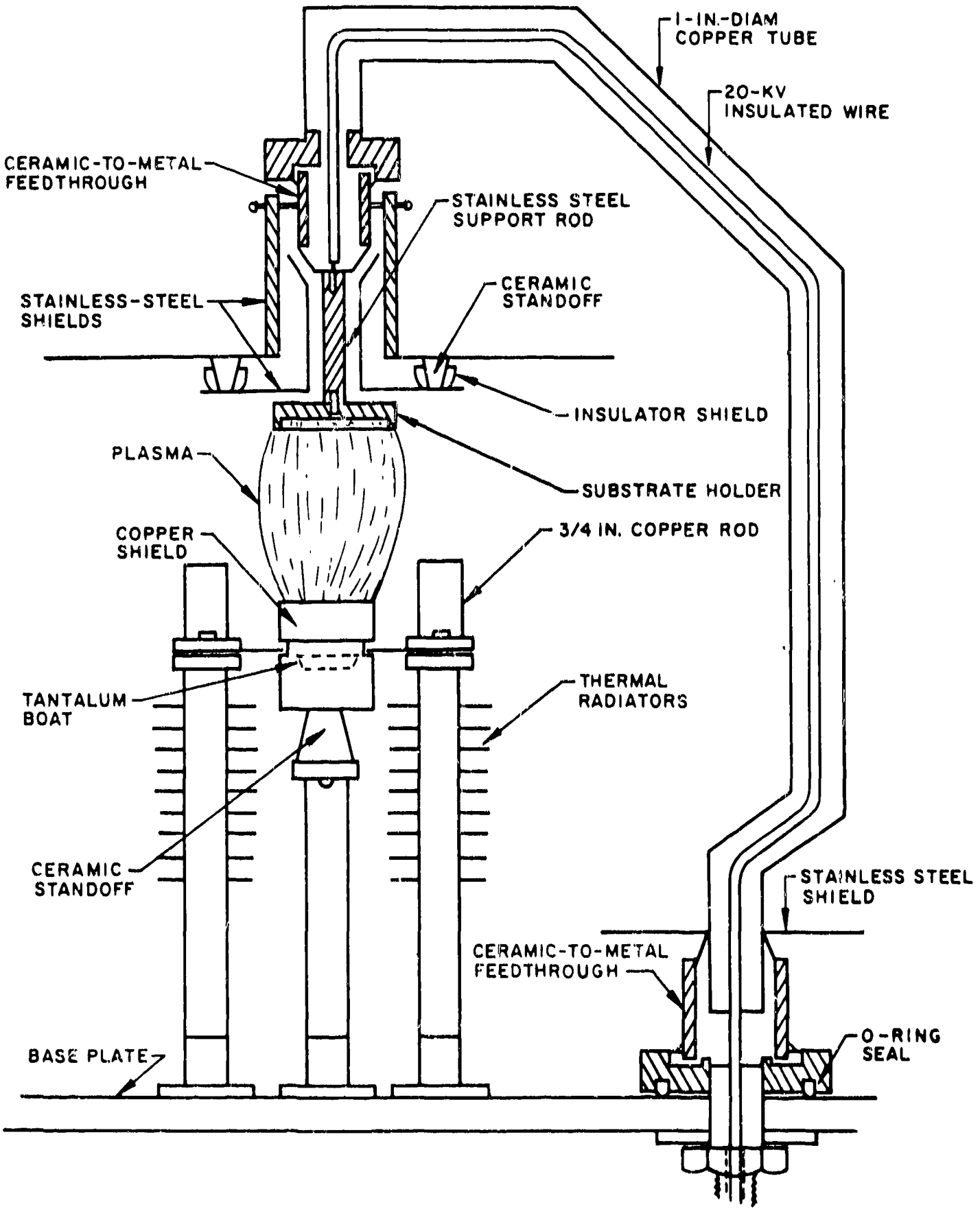

Fig. 3.3--First cathode assembly

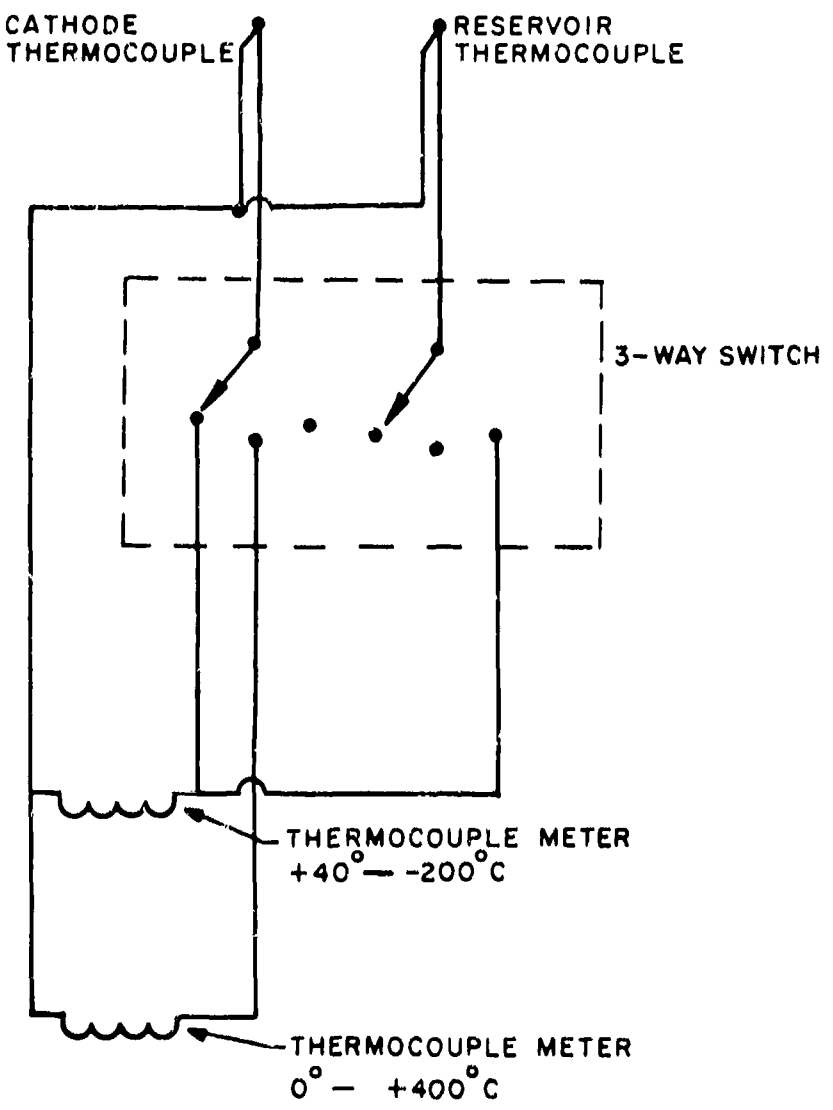

Fig. 3.4--Cathode-assembly temperature-monitoring system

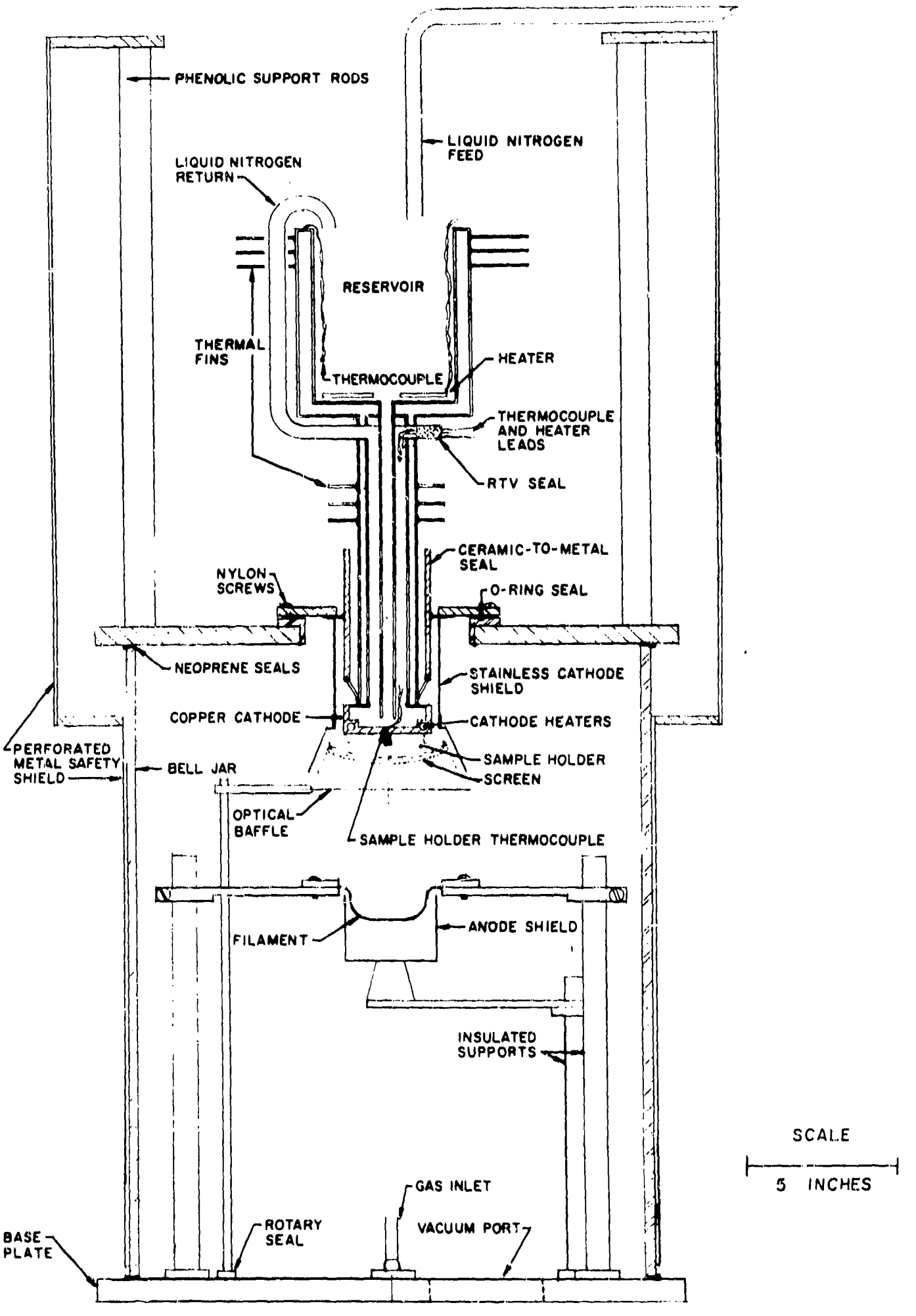

Fig. 3.5--Ion-implantation system with cooled substrate holder

Both cathode assemblies must be cleaned periodically. When an abnormal discharge occurs, it usually is an indication that the assembly needs to be cleaned. When abnormal breakdown does occur, the high-voltage cathode power supply will indicate an overcurrent condition. This type of breakdown happens much too fast for the current regulator system, previously mentioned, to respond; repeated abnormal discharges can perforate the electrostatic shields. All metal parts are cleaned with water and alcohol. The ceramic parts are cleaned of all metal that has been deposited.

After each run, the cathode assembly is heated to expel the water that condenses inside the reservoir. Failure to do this will result in the cooling system becoming plugged with ice during the next cooling cycle.

Two thermocouple meters mounted inside the high-voltage section are used to measure the temperature from -200° C to +400° C. An insulated switch is provided to change scales. There are two thermocouples mounted on the cathode assembly; one measures the temperature on the back face of the sample holder and the other monitors the temperature inside the liquid nitrogen reservoir and provides a crude measurement of the liquid nitrogen level.

The physical shape of the sample holder determines to a large degree the plasma form and the implantation rate. Several different types of sample holders have been used. The uniformity of the implantation can be determined by visually inspecting the plasma shape. The implantation will be thickest where the plasma intensity is greatest. Two types of sample holder that have been used with success and the shape of the plasma are shown in Fig. 3. 6. Intensifiers may be added at points where the plasma is weak. The intensifiers provide secondary electrons in localized areas and thus intensify the plasma in those areas.

3. 6. METAL EVAPORATION

After a stable, localized plasma is achieved, the metal to be implanted must be injected into the plasma by evaporation. The evaporation of most metals is a straightforward process. Some metals, however, are not easily evaporated. Aluminum, which is used for implantation of semiconductors and insulators, is particularly troublesome to evaporate. Several weeks were spent trying to develop a continuous source of aluminum which could be used for extended periods of time. The electron bombardment technique would be useful in a straight evaporation process, but it is not suitable for ion implantation because of the presence of the plasma and the high partial pressure of argon.

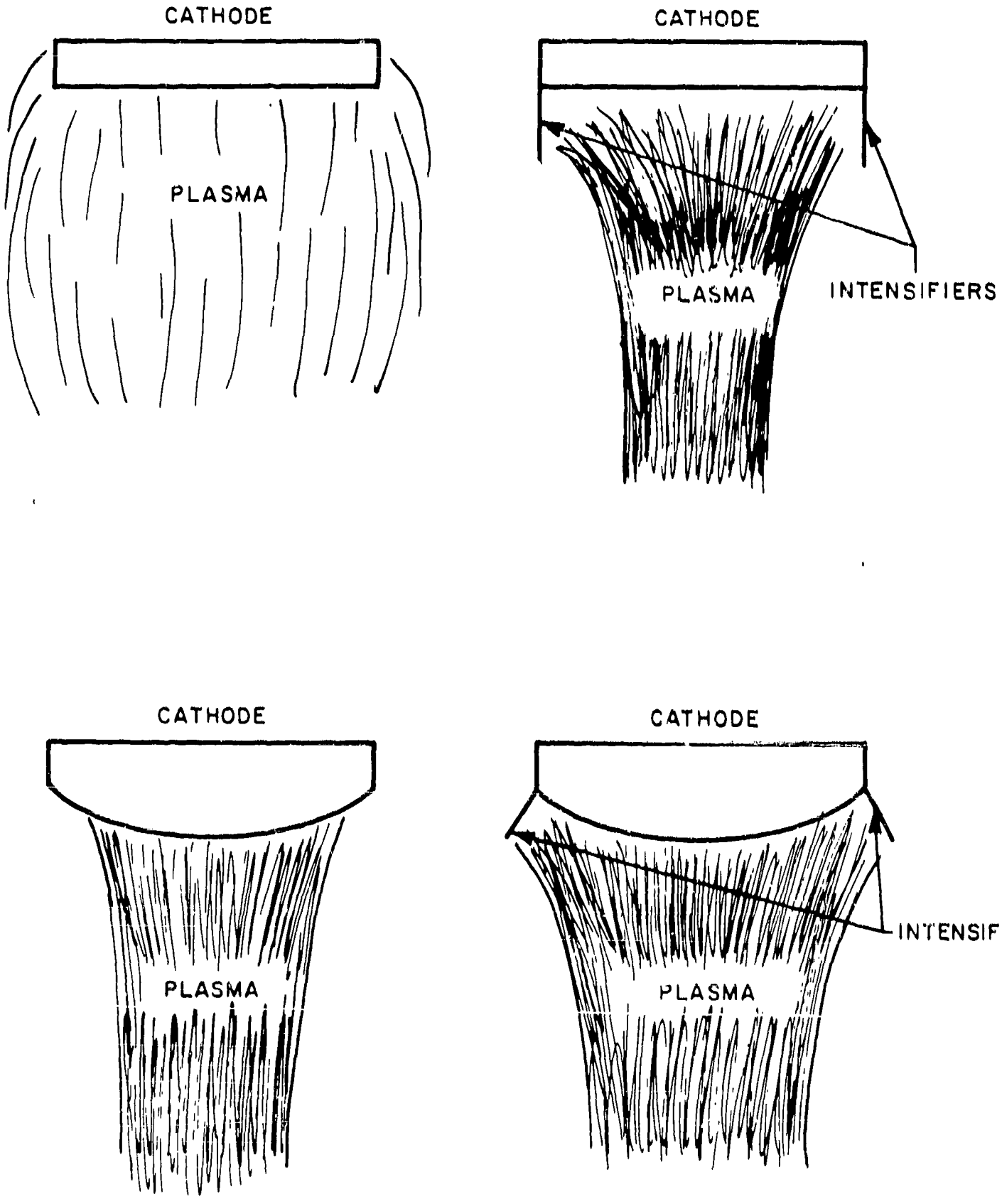

Fig. 3.6--Cathodes with and without intensifiers

Tungsten and tantalum boats were the first type of boats tried. These boats proved to be unsatisfactory for evaporation of aluminum. The aluminum etched the boat and large holes were formed during the first minute of evaporation. Several other materials were tried, including boron nitride, alumina, and graphite. These, too, were found to be unsuitable. It was finally determined that tungsten filaments were the best available method for aluminum evaporation. These filaments have to be loaded with aluminum at the beginning of each run. The filaments also have to be changed after every three or four evaporation runs. Commercial filaments were found to be less versatile than those which could be made in the laboratory. Tungsten wire with a 0.06 in. diameter is easily formed into the desired filament shape. The filament shown in Fig. 3.7 has the longest filament life. This configuration was also designed to approximate a plane source as a plane source provides a more uniform deposition than a point source; in addition, more uniform heating of each strand of the filament is attained with this design. Soft aluminum is cut and formed into small hooks which are placed on the flat section of each strand. When the aluminum melts, the surface tension causes it to ball up and hang from the filament. The molten ball will then spin about the axis of the strand and run back and forth along the flat section of the strand. This approximates four line sources in a plane. Because the ball runs along the strand, the tungsten is etched more uniformly, thus giving a much longer filament life. As shown in Fig. 3.8, the filaments are shielded to prevent coating the vacuum walls. A mirror placed as shown allows one to observe the filament.

Nickel and nichrome exhibit the same characteristics as aluminum when they are evaporated from refractory metal boats or filaments. These metals, however, can be evaporated from refractory metal boats with alumina and boron nitride coatings. Boats of this type are commercially available.

Metals such as copper and gold do not work well with filaments because of their low surface tension in a molten state. Tantalum boats are suitable for such metals. Tantalum boats are easily formed from 10-mil tantalum sheet.

If a high partial pressure of a noble gas is used for the evaporation, some of the equipment in the chamber will be coated with an amorphous black material; sometimes this also occurs during implantation. A spectral analysis has shown that this black soot is a pure amorphous form of the evaporated metal.

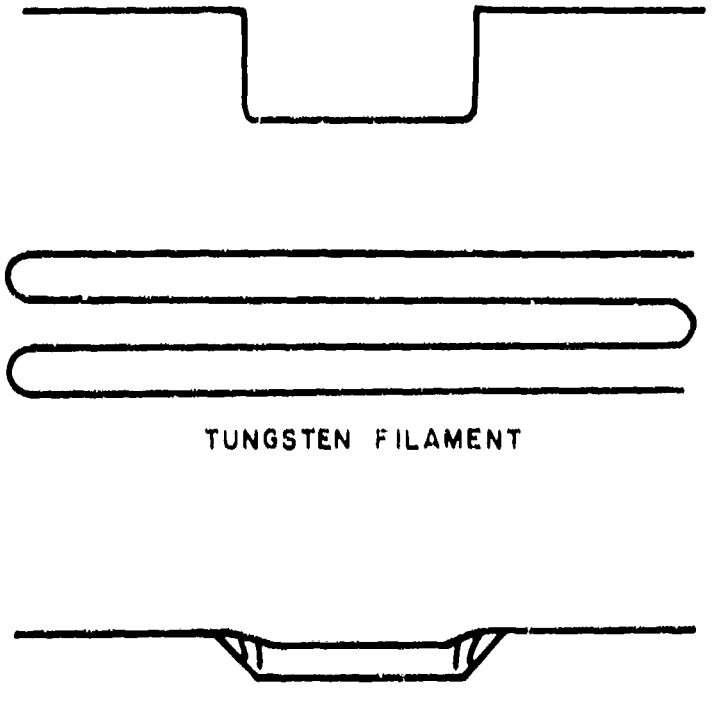

Fig. 3.7--Evaporation heaters

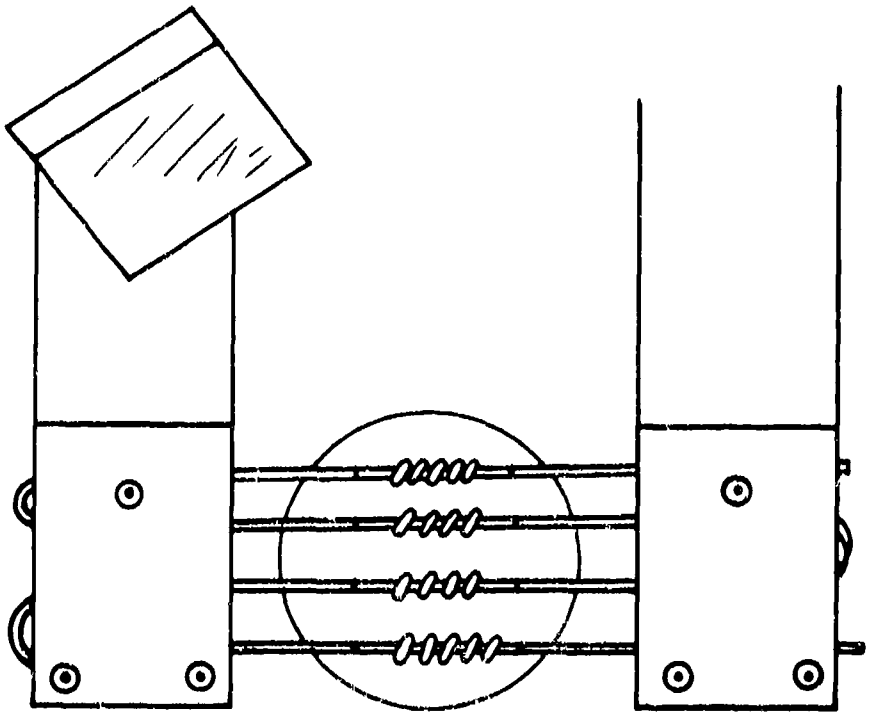

TOP VIEW

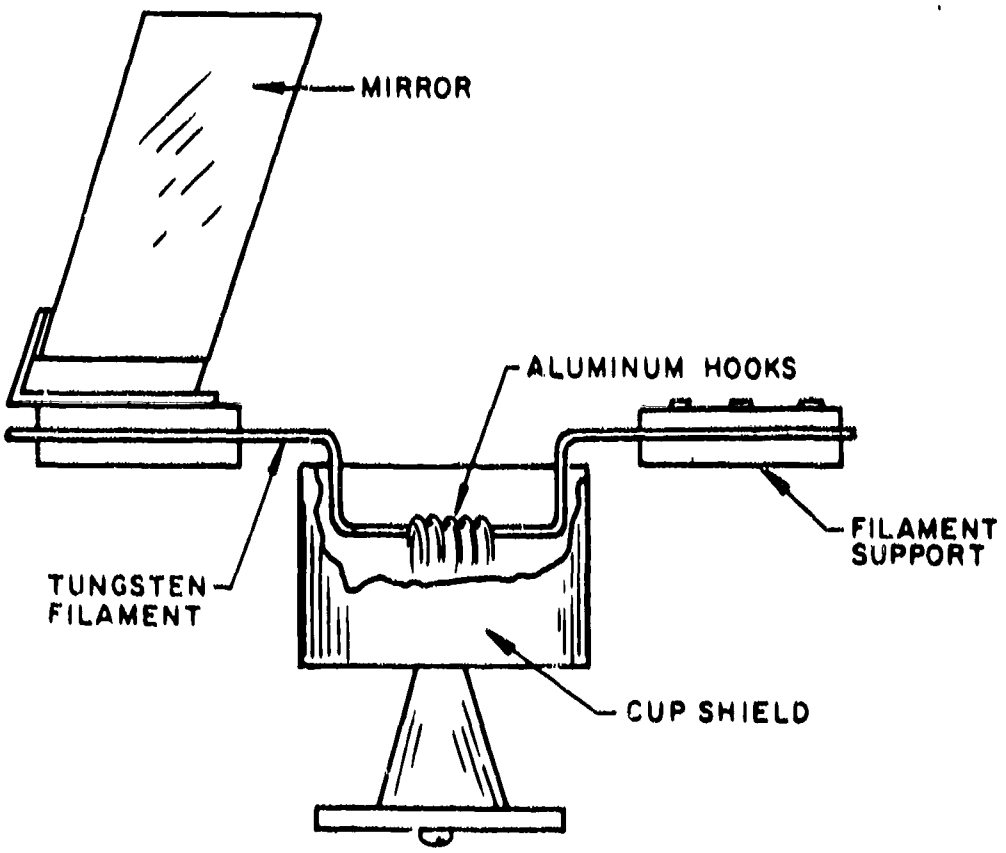

SIDE VIEW

Fig. 3.8--Aluminum vapor source

3. 7. MONOENERGETIC ION SOURCE

To obtain deeper penetration and higher-energy metal ions, a conventional ion source was designed and built. The metal ions are created inside the source and extracted. These ions then fall through the full cathode potential. A noble gas is not required to sustain this source.

A pure aluminum plasma is established inside the source by using an energetic electron source, a neutral aluminum vapor, and appropriate electric and magnetic fields to enhance the ionization process. By optically shielding the aluminum vapor source, a low neutral efflux is maintained. Other metals can be used for the vapor source if desirable. Electrons emitted from a hot tungsten filament are accelerated and injected into a field-free region. A magnetic field of about 400 gauss is directed normal to the direction of the electron line of flight. Aluminum evaporated into this region is ionized by the orbiting electrons. Aluminum ions drift out of the field-free region and are extracted past the electron emitter into the chamber. These extracted ions then fall through the full cathode potential and are implanted into the substrate mounted on the cathode. With the source configuration shown in Fig. 3. 9, a 30-mA beam can be maintained for approximately 2 min.

By leaking in argon, the source can be run on the residual argon. A partial pressure of 4×10^{-4} torr is required. At this pressure, the mean free path of the argon ion is well over 1 meter. This fact assures that the ions are monoenergetic and have not experienced any collisions during their flight between the source and the cathode. This monoenergetic argon ion source can be used to clean the substrate surface prior to implantation of the metal.

This ion source has been run several times with no apparent problems. This type of monoenergetic ion source has many experimental advantages over the plasma source. Because the metal ions are monoenergetic, the energy and depth of penetration may be controlled to produce more consistent results. The absence of the plasma eliminates most contaminant sputtering and subsequent implantation. The possibility of using this source for general production of samples is questionable.

3. 8. ION IMPLANTATION ON MYLAR

Metals, insulators, and semiconductors have all been successfully implanted with ionized metal. Implanted metal surfaces have been soldered and spot-welded with reasonable success, and ohmic contacts have been made on high-resistivity semiconductors.

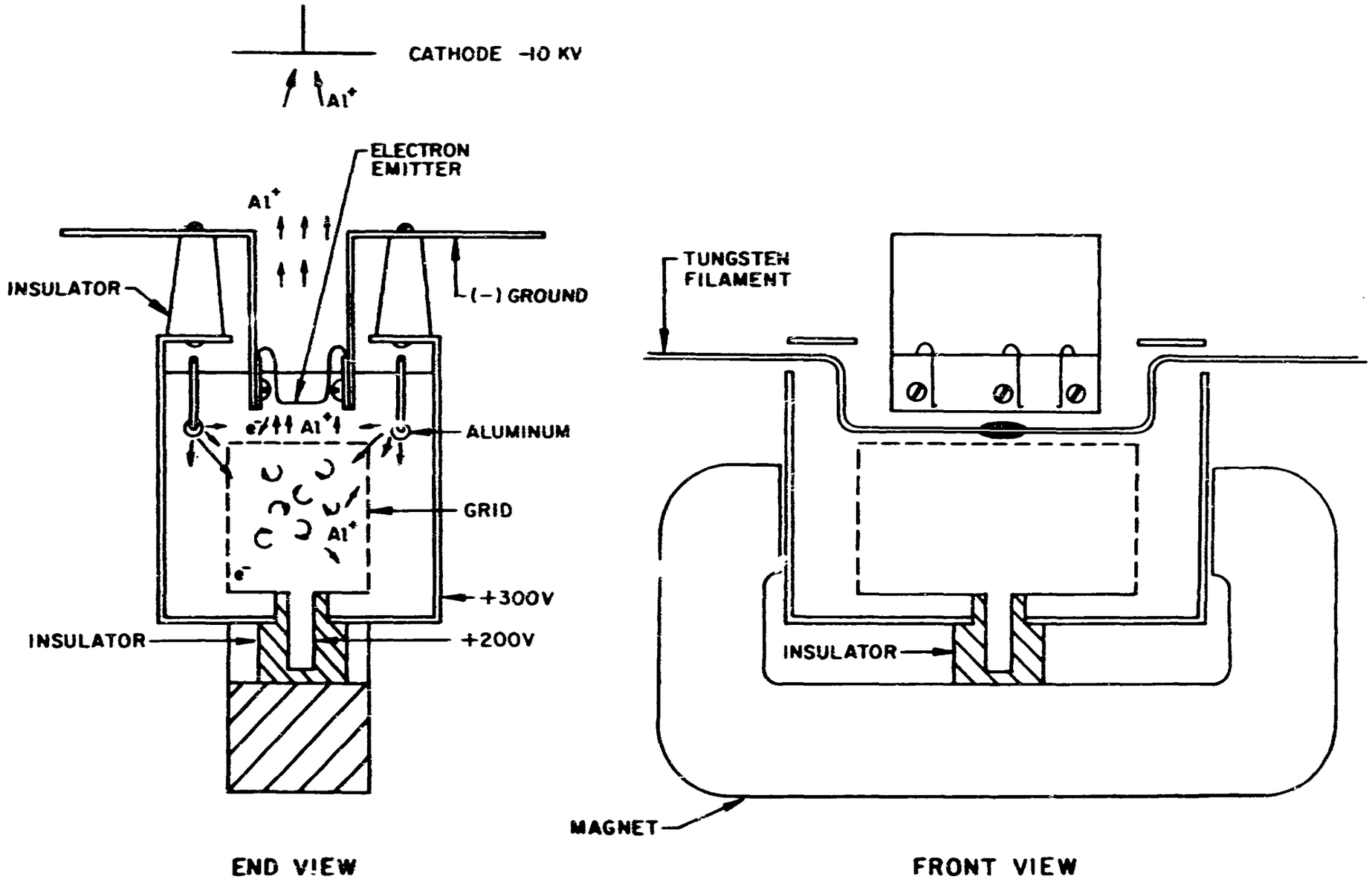

Fig. 3.9--Ion source

Implanting metal ions in insulators is the most difficult of the three types of substrates. Because of the low thermal conductivity associated with insulator materials, the exposed surface and implanted film may become very hot. The low electrical conductivity results in a large surface-charge buildup. Arcing across the surface film during the implantation will burn holes in the film and insulators.

Glass, quartz, mica, and Mylar have been implanted with aluminum and copper. The general information for establishing the plasma and the cleaning procedures are all applicable to the process of insulator implantation. Most of the problems arise at the surface of the sample. To reduce the problem of high surface temperatures, lower power levels are used in the implantation of the metal. The substrate holder is usually cooled to a low temperature prior to starting the plasma. To reduce the surface charge, a screen is mounted over the sample about 0.25 in. from the surface. This screen is at the same potential as the cathode. The purpose of this screen is to establish an equipotential surface in front of the substrate. The screen will produce many secondary electrons due to the ion bombardment. These electrons will tend to neutralize the positive charge on the surface of the insulator. The screen also reduces the number of secondary electrons which leave the surface of the insulator. Some neutral flux and some ions will reach the insulator even if the screen is absent. It will be observed, however, that as the conductive film begins to form, arcing across the surface will occur. When one point of the film touches the mask or any part of the cathode, the surface charge will rush to the point of contact and subsequently burn the film and insulator. It has also been found that if both sides of a thin dielectric are to be implanted, the front, or first, side of the film must be insulated electrically from the cathode when implanting the reverse side. Mica was implanted on both sides, and it was found that the front side of the film would burn and pit when the reverse side was implanted. The reverse side was obviously in a cooler environment as it was pressed against the sample holder, but yet it was destroyed each time. When Mylar was implanted, large holes would be torn in the Mylar when implanting the second or reverse side. The substrate would remain intact until the initial metal began to implant itself into the Mylar. It was apparent that the problem is electrical in nature. It is not yet clear why the phenomenon occurs. The problem was eliminated by placing a 1-mil sheet of Mylar between the substrate holder and the dielectric sample when implanting both sides.

Using the above information, most insulators can be implanted with a tough adherent film. Mylar, because of its low melting point, required some additional techniques to successfully implant it. The sample holder for Mylar is made of aluminum in the shape shown in Fig. 3.10. The Mylar film is stretched over the curved face and spring-loaded. Loops

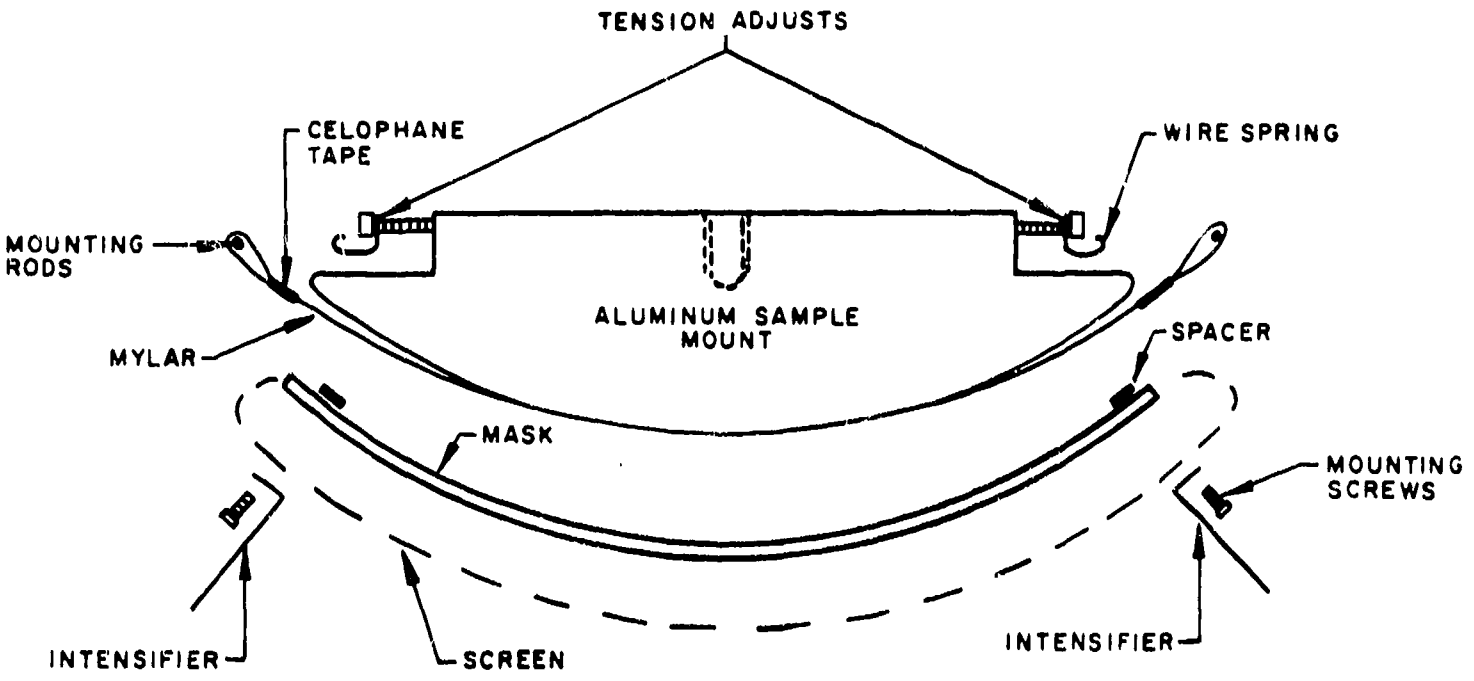

Fig. 3.10--Mylar sample mount

are made at each end of the Mylar strip, as shown. Ordinary cellophane tape is quite suitable for this. A thin rod is placed through each loop (as shown) and hooked by the two spring wires. The exposed surface is cleaned with ethyl alcohol. The aluminum mask is placed over the surface but does not touch the Mylar. The screen is placed over the mask and the intensifiers are fitted at each end to provide a uniform deposition. This unit is then screwed tightly against the cathode. Two shields are slipped down around the Mylar sample holder to limit the plasma to the surface only. The sample holder is heated to 150° C during the pump-down. This anneals any small wrinkles and helps to clean the surface of the Mylar. After the pressure is below 1×10^{-5} torr, liquid nitrogen is pumped into the cathode reservoir. After about a 5-min delay to allow the sample holder to reach equilibrium, the cleaning process is started. The cathode voltage is initially set at 6, 000 V. When a current density of 0. 3 mA per square centimeter is maintained by adjusting the argon pressure, the cathode voltage is 3, 200 V, owing to the voltage drop across the stabilizing resistor and the voltage decrease in the power supply. A cleaning period of about 30 min is required at that power level to clean the surface of the Mylar. After this cleaning period, the aluminum is introduced into the argon plasma. The implantation can be observed. An initial tan hue will first appear. This quickly changes to the metallic color of aluminum. After the implantation has covered the surface, the pressure can be reduced rapidly by shutting the manual control valve for the argon leak. The plasma will reduce in intensity and stop and the surface will continue to be coated but with an evaporated film. The substrate holder is then heated back up to 150° C. This anneal eliminates the wrinkles that formed due to the aluminum coating. The process is repeated for the reverse side, but care must be taken to insulate the aluminized surface from the cathode.

3. 9. CONCLUSION

The results of this work have shown that ion implantation can be used as a very effective technique for plating various surfaces. Although the methods described here have been quite successful, simpler techniques will probably evolve with continued investigation. The ion-plating system has proved to be quite functional.

4. TRANSIENT RADIATION EFFECTS IN MYLAR VERSUS TEMPERATURE

The data in Table 1 were taken during irradiation of a Mylar capacitor from liquid nitrogen temperature (LN) up to room temperature and were reported in the fourth quarterly report.[2] The delayed conductivity signals were analyzed into the individual exponential components listed. It was noted that the time constants of the two shortest components (~6 μsec and ~ 40 μsec) were essentially independent of temperature, although the magnitudes of the components indicated fairly strong temperature dependence. Carrier lifetimes in the conduction band in insulators are usually orders of magnitude shorter than the observed decay times. Therefore, recombination processes occur after the carriers, electrons for example, are trapped and thermally untrapped many times before recombining with holes at recombination centers. At room temperature, the decay of the radiation-induced conductivity was fitted to a hyperbolic form, indicative of direct recombination, only out to 100 μsec. It seems most reasonable to attribute the observed response to a continuous distribution of traps in the forbidden zone in addition to the relative immobility of one sign of carrier. Under these conditions it is possible to have an observed time constant which is relatively insensitive to temperature and a photocurrent which increases slowly with temperature,[9] as displayed in Mylar. It is necessary, according to this model, that the rate of exchange between conduction electrons and trapped electrons be large compared to the rate of exchange with recombination centers. The recombination centers or primary centers can be a factor of 10^8 larger than the number of electrons in the conduction band and a desensitizing effect is observed in which the photocurrent is reduced to 10^{-8} times the photocurrent in the absence of trapping. Since replenishment of carriers in the conduction band from the traps takes place during the recombination process, the observed time constant is considerably longer than carrier lifetime. In this model $\tau_0 = 10^{-1} \tau n_p / n_c$, where τ_0 is the observed delay time, τ is the average carrier lifetime, n_p is the number of trapped holes ($\sim 10^{15}/cm^3$), and n_c is the number of conduction electrons (10^7 to $10^{15}/cm^3$). In the absence of replenishment, the observed time constant is much shorter. Depending on trap depths, both decay time constants may occur in the same specimen, leading to observation of long and short components in the decay curve. Thus, it is reasonable that the entire decay curve could be analyzed into several components with time constants which were insensitive to temperature.

Table 1

DELAYED CONDUCTIVITY COMPONENTS

Temp. (°K)	Σ/V_0	V_p/V_0	τ_1 (μsec)	V_1/Σ	V_1/V_0	τ_2 (μsec)	V_2/Σ	V_2/V_0	τ_3 (μsec)	V_3/Σ
293	2.9×10^{-2}	2.1×10^{-2}	14	0.12	3.5×10^{-3}	104	0.13	3.7×10^{-3}	950	0.02
293	2.2×10^{-4}					43	0.10		240	0.05
93	1.36×10^{-2}	1.32×10^{-2}	6.1	0.009	1.2×10^{-4}	41	0.02	2.7×10^{-4}		
123	1.49×10^{-2}	1.42×10^{-2}	5.7	0.025	3.7×10^{-4}	41	0.023	3.4×10^{-4}		
193	1.54×10^{-2}	1.41×10^{-2}		--	--	40	0.057	8.8×10^{-4}		
223	1.66×10^{-2}	1.59×10^{-2}	6.7	0.024	4.0×10^{-4}	50	0.078	1.3×10^{-3}		
273	1.88×10^{-2}	1.54×10^{-2}	5.8	0.069	1.3×10^{-3}	54	0.111	2.1×10^{-3}		

Note: Σ = asymptotic value of signal voltage.
V_0 = applied voltage.

The reduction in photocurrent at the end of the experiment compared to the original value at room temperature is evidence of deep carrier traps which were filled during the irradiation at the low temperatures and which were not thermally emptied as the temperature was raised back to room temperature. This effect has been observed in other insulators that again displayed the original photocurrent at room temperature after the samples had been heated.[10]

It is somewhat presumptuous to apply band models to Mylar, which does not resemble the inorganic crystalline solids usually associated with such models; however, the behavior of the observed response may be fitted to such models and therefore they are of value until additional experiments lead to more definitive models.

5. LINAC TESTS OF CERAMIC AND GLASS CAPACITORS

Linac irradiations of two new types of capacitors were performed to see if a significant improvement in transient radiation response was evident. Only one sample of each type was tested as this was only a survey to determine whether further testing would be desirable. Irradiation exposure rates of 10^7 to 10^9 rads (Cu)/sec were employed.

The ceramic capacitor has a capacity of 0.1 μF at a working voltage of 100 V. Thin films of ceramic and electrode material are fused into a monolithic solid that is 0.3 in. by 0.3 in. by 0.1 in. in size. The large temperature coefficient of these high-dielectric-constant ceramic formulations, which have a ± 15% change in capacity over the temperature interval -55 °C to 125 °C, limits their use to noncritical circuit applications. No delayed conductivity was observed with 4-μsec Linac pulses. The prompt coefficient, K_p, was calculated from the expression $I = K_p V C \dot{\gamma}^{\Delta}$, where V is voltage applied in volts, C is capacity in farads, $\dot{\gamma}$ is the exposure rate in R/sec, Δ is a constant between 0.5 and 1.0, and I is the prompt current in amperes. The resulting value, $K_p = 1.1 \times 10^{-6}$, is comparable with previously measured monolithic capacitors from another manufacturer.[11]

Two glass capacitors from Corning Glass Works were irradiated, one of which--a conventional type with a 0.01-μF capacity--has been available for several years. It has a temperature coefficient of 140 ppm over the temperature range -55 °C to 125 °C, resulting in less than ±2% capacity change over this temperature interval. It is a stable capacitor, having a dielectric constant of about 8.4. The second glass capacitor has a dielectric called Glass-K. Three formulations of this material are available with dielectric constants up to two orders of magnitude larger than that of ordinary glass. This high dielectric constant is achieved through heat treatment of the glass, which forms microcrystals throughout the dielectric. As the dielectric constant is increased, the temperature stability decreases, as with ceramic dielectrics. Table 2 lists the maximum capacity available with each temperature stability characteristic over the temperature range -55 °C to +125 °C. All the listed capacitors have the same physical size--0.25 in. long by 0.14 in. diameter.

Table 2

Maximum Capacitance (μF)	Stability Characteristic	Temperature Coefficient, (%)
0.02	T	+2, -10
0.039	U	+2, -15
0.100	V	+10, -40

Samples having U and V characteristics were ordered, but the 0.1-μF, V-type capacitors arrived too late for testing. Under the same test conditions as those used for the ceramic capacitor, the prompt coefficient for the ordinary glass capacitor was $K_p = 4.5 \times 10^{-7}$ and for the Glass-K capacitor with 0.039 °F capacity and stability characteristic U it was $K_p = 2.3 \times 10^{-7}$. No delayed conductivity was observed with 4-μsec Linac pulses. It is possible that the dielectric formulation with characteristic V would have an even smaller K_p; however, its wide temperature stability tolerance would prevent its use in critical circuits in the same way that ceramic capacitors are limited.

6. ENERGY LOSS OF MODERATELY FAST ELECTRONS IN INSULATORS

6.1 INTRODUCTION

Electron energy loss in materials is a process that has been studied extensively; however, little attention has been given to the later stages of the process.[12] In order to obtain better numerical estimates for the theory of transient radiation response discussed in a previous report,[1] the slowing down of electrons whose energy is 100 eV or less is examined in detail. It is assumed that the Bethe theory, based on electronic excitations, is sufficient to give the range down to this energy. Thus, the mechanisms whereby an electron transfers energy to those excitations in a solid which have low energy are treated here.

The Hamiltonian for the undisturbed solid contains terms which give rise to all of the excitations that can exist in the solid. It is not necessary to write down this Hamiltonian but merely to list the types of excitations that are known to exist and their approximate energy: acoustic phonons (0 to 0.03 eV), optical phonons (0.03 eV), dipolar relaxation (characterized by a time τ_d, with $0 \leq \hbar/\tau_d \leq 0.03$ eV), excitons (2 to 10 eV), band-to-band electronic transitions (2 eV and greater), and plasmons (15 eV). There are also interactions between these excitations.

The term solid in the above context is usually taken to mean a perfect crystal. It is fair to say that this is because the mathematics are thereby simplified rather than because the phenomena are different. For example, there is probably not much difference in the range of a fast electron in a solid metal or a liquid metal or, more appropriate for the problem at hand, in quartz or glass. Thus, the term solid is extended to mean any dense material, which, in this context, includes organic

polymers and liquids. Of course, the initial testing of the theory will best be done in a well-understood material, i.e., in a perfect crystal.

A crude estimate is made of the contribution of various loss mechanisms for an energy low enough that band-to-band and plasmon excitations are not important. It is found that the losses to excitons and to acoustic phonons dominate.

6.2 MATHEMATICAL DETAILS

The method used here to treat the problem is to relate the energy loss of the electron to the imaginary part of the dielectric constant (which in turn gives the energy loss of a photon propagating through the crystal). This method has been fruitful in studying the energy lost to collective plasma oscillations.[13] It is fitting to note, however, that this method was first used in a problem akin to the one studied here.[14]

If an extra electron is added to the solid, there will be a coupling between the excitations listed above and the charge. For those excitations that involve only electrons, the coupling can be written most easily in terms of the interaction energy of two charge densities. The charge density of the electrons in the solid, in terms of its Fourier coefficients in space, is $-e\rho_k$. The charge due to the extra electron, written in terms of its Fourier coefficients in space and time, is $-e\sigma_{k\omega}e^{i\omega t}$. (Conventionally, this interaction is considered to be turned on slowly from $t = -\infty$ by some factor $e^{\delta t}$, with $\delta \to 0$. As this is considered to be a device employed to ensure that the correct contours will be taken when doing the Fourier integrals, this factor is, for convenience, omitted. The subscripts on σ are also omitted.) The form[15] of the electron interaction is

$$H_e = \sum_k \frac{4\pi e^2}{k^2}\left(\rho_k + \sigma e^{i\omega t}\right) . \qquad (1)$$

Now consider the energy of interaction with the optical phonons. The optical phonons will, in general, be accompanied by a polarization

of the molecules. The strength of the mode of wave vector k is labeled $Q_j(k)$, where j stands for both the vector component of the displacement and the type of mode. A phenomenological relation between the i^{th} component of the macroscopic electric polarization M_i and the optical mode Q_j is assumed; this relation has the form

$$M_i = eM_{ij}Q_j \ . \tag{2}$$

The convention that repeated indices are to be summed will be followed. It should be noted here that M has been used to denote polarization; the symbol P, which is commonly used for polarization, will be employed for a different quantity. The extra energy that exists when a field $\vec{E}_{ex}(r)$ generated by the extra electron is applied and the material has a polarization $\vec{M}$ is

$$H_{ph} = \int \vec{E}_{ex}(r) \cdot \vec{M}(r)\, d^3r = \sum_k \vec{E}_{ex}(k) \cdot \vec{M}(k) \ . \tag{3}$$

The field generated by the extra charge σ must satisfy Poisson's equation

$$i\vec{k} \cdot \vec{E}_{ex}(k) = -4\pi e\sigma \ . \tag{4}$$

Further, if the retardation effects are ignored, the field is longitudinal (along $\vec{k}$), so the solution to Eq. (4) is

$$\vec{E}_{ex} = i\frac{\vec{k}}{k^2} 4\pi e\sigma \ . \tag{5}$$

The use of Eq. (5) for $\vec{E}_{ex}$ allows Eq. (3) to be written in much the same form as Eq. (1). Thus, the total interaction found so far can be described in terms of a more elaborate charge operator:

$$P_k = \rho_k - ik_i M_{ij} Q_j^+ \tag{6}$$

and thus

$$H_{int} = H_e + H_{ph} = \sum_k (4\pi e^2/k^2)\, P_k^+ \sigma e^{i\omega t} \ . \tag{7}$$

If molecules in the solid have a permanent dipole moment, it can be included formally as a zero-frequency phonon mode. If this dipole moment has two (or more) stable positions, two or more zero-frequency modes can be used. The transitions between these modes give rise to the dipole losses.[16,17]

There is one other loss mechanism that occurs -- the coupling to acoustic phonons. It may be that this mechanism appears such a low energy that it is not of interest--i.e., by the time an electron's energy drops to kT, it may be meaningless to inquire into its range from that point on; even so, it should be mentioned for completeness. The deformation potential model, which is valid for semiconductors, will be used.[18,19] Here, the interaction is assumed to be proportional to the strain, which in turn is the derivative of the displacement. The displacement of the acoustic modes, which carry no polarization, is labeled $\vec{q}$. The interaction energy will be

$$H_{ac} = + \sum_{k} (4\pi e^2/k^2)\, \xi_{ij} i k_i q_j^+ \sigma e^{i\omega t} , \qquad (8)$$

where ξ_{ij} is the deformation potential tension that is set up when an electron is present. ξ_{ij} has been normalized somewhat differently than usual so that it will fit the standard format used.

The coupling between the electron and the various excitation modes of the solid have now been obtained in Eqs. (7) and (8). There is now the problem of calculating the energy transferred (or lost) from the electron to the solid. The easiest way to calculate this energy loss is to calculate the probability that the solid has been excited from its initial state, 0, to a state n. Conservation of energy then ensures that the electron has lost energy $E_n - E_0 = \hbar\omega_{n0}$. That the expression for energy loss is identical to a certain expression involving the dielectric constant remains to be shown.

The energy loss, $W(k\omega)$, will be found here without formal proof. This will be done because the answer can be essentially copied out of Pines.[15] The difference is that where Pines treats a problem with the single operator ρ_k^+, the sum

$$P_k^+ + ik_i \xi_{ij}^* q_j^+ . \tag{9}$$

is used here. Thus, Pine's "golden rule" result and the generalized interaction derived here is written as

$$W(k\omega) = \frac{2\pi}{\hbar^2}\left(\frac{4\pi e^2}{k^2}\right) \sum_n |(P_k^+ + ik_i \xi_{ij}^* q_j)_{n0}|^2 \, \delta(\omega - \omega_{n0}) . \tag{10}$$

Actually, Eq. (10) probably requires considerably more justification than given here. In the first place, it is based on the assumption that the electron is sufficiently localized in space that it has a uniform momentum density. In other words, we have set $|\sigma|^2 = 1$. It is conceivable that at the lower energies, the wave packet describing the electron will be spread out so much that $|\sigma|^2$ must be a not-so-slowly-varying function of k. A second point that must be checked is whether the interactions are indeed weak enough that only the first term in the perturbation series can be retained. Assuming this will be done in the future, Eq. (10) will be accepted as valid for the moment.

For convenience later, Eq. (10) is written in a slightly different form. Q, q, and ρ are all boson operators. This means, for example, that $(q_j^+)_{n0}$ is zero unless the only difference between state n and state 0 is that n contains one more acoustic phonon of type j. It is assumed that the wave functions can be written as a product of states containing acoustic phonons (labeled β) and states containing optical phonons and electronic excitations (labeled α) Thus, Eq. (10) can be written in two parts:

$$W(k\omega) = 3\pi \left(\frac{4\pi e^2}{\hbar k^2}\right)^2 \left\{ \sum_\alpha |P_k|^2 \, \delta(\omega_{\alpha 0} - \omega) + \sum_\beta |(ik_i \xi^*_{ij} q_j^+)_{\beta 0}|^2 \delta(\omega_{\beta 0} - \omega) \right\} . \quad (11)$$

Now, the calculation of the dielectric constant, ϵ, can be considered. If a polarization such as $\vec{M}$ is present, $\vec{E}$ must satisfy Poisson's equation, in which the source of $\vec{E}$ is all of the free charge minus the divergence of $\vec{M}$,[20]

$$i\vec{k} \cdot \vec{E}_k = -4\pi [e(\rho + \rho_{ext}) + i\vec{k} \cdot \vec{M}_k] . \quad (12)$$

In Eq. (12), ρ_{ext} is the external charge used to establish a field to probe the solid. The definition of $\epsilon(k\omega)$ is that $\epsilon\vec{E}$ obeys a Poisson equation in which only the external charge appears; thus,

$$\epsilon i\vec{k} \cdot \vec{E}_k = -4\pi e \rho_{ext} . \quad (13)$$

Equations (12) and (13) may be combined to yield

$$\frac{1}{\epsilon} = 1 + \frac{\rho + e^{-1} i\vec{k} \cdot \vec{M}}{4\pi \rho_{ext}} , \quad (14)$$

or, in terms of the operator P defined in Eq. (6),

$$\frac{1}{\epsilon(k\omega)} = 1 + \frac{P_k}{4\pi \rho_{ext}} . \quad (15)$$

The value measured for $1/\epsilon$ will depend on $(P_k)_{pp}$, where p is the ground state of the solid in the presence of ρ_{ext}.

Again, this is exactly the same equation as Pines obtains for $1/\epsilon$.[15] Thus, a solution for $(P_k)_{pp}$ may be expected to follow the same formal steps as employed by Pines, so that

$$\mathrm{Re}(1/\epsilon) = 1 + \frac{4\pi e^2}{\hbar k^2} \sum_\alpha |(P_k^+)_{\alpha 0}|^2 \frac{2\omega_{\alpha 0}}{\omega^2 - \omega_{20}^2} , \quad (16)$$

$$\mathrm{Im}(1/\epsilon) = \frac{4\pi^2 e^2}{\hbar k^2} \sum_\alpha |(P_k^+)_{\alpha 0}|^2 [\delta(\omega - \omega_{n0}) + \delta(\omega + \omega_{n0})] . \quad (17)$$

The last term in Eq. (17) represents a gain of energy by the field, i.e., stimulated emission. If the solid is at zero temperature, such processes would be impossible (i.e., $\omega_{n0} > 0$ for all n). Even at elevated temperatures, the number of such processes should be small enough that they can be ignored.

A comparison of Eq. (11) for the energy loss with Eq. (17) for $\mathrm{Im}(1/\epsilon)$ allows the expression for energy loss to be written as follows:

$$W(k\omega) = -\frac{8\pi e^2}{\hbar k^2}\,\mathrm{Im}\left(\frac{1}{\epsilon(k\omega)}\right) + 2\pi\left(\frac{4\pi e^2}{\hbar k^2}\right)\sum_{\beta}\left|\left(i\,k_i \xi^{*}_{ij} q^{+}_{j}\right)_{\beta 0}\right|^2 \times \left[\delta(\omega_{\beta 0} - \omega) - \delta(\omega_{\beta 0} + \omega)\right]. \qquad (18)$$

According to Eq. (18), there is a term in the energy-loss expression that is not given by the dielectric constant. This is because, as stated previously, the acoustic modes are not accompanied by a polarization of any sort, so the externally generated field is not coupled to these modes. If this is correct, it is logical to ask why the electron is coupled to them. The answer is that the allowed energy levels depend on the position of the atoms. Any change in the position, be it a uniform compression or an acoustic wave, induces a change in the energy of the electrons. The electrons can follow the lattice adiabatically so an electric field is never generated during the process. The proof (or disproof, as the case may be) of the above statements is an interesting physical problem. As mentioned before, it is not clear whether this process affects the total range of the electron but it is most important at very low energies.

6.3 FORMULA FOR LINEAR RANGE

If Eq. (18) is accepted for the energy loss, a large part of the problem is solved conceptually. Much detailed analytic work remains,

however, before the range can be found. As a first step, let us find the linear range. This is given, in the continuous method, by the expression[21]

$$R = \int_{E_f}^{E_0} \frac{dE}{-dE/dx} \tag{19a}$$

In Eq. (19a), E_0 is the initial energy and E_f is the final energy. The energy loss per unit range, dE/dx, is found from the energy loss per unit time, dE/dt, by

$$\frac{dE}{dx} = \frac{1}{v}\frac{dE}{dt} \tag{19b}$$

where v is the velocity. Now W is the probability of losing energy $\hbar\omega$ and momentum $\hbar k$ per unit time per unit volume in k space; thus the expectation (mean value) of the energy loss per unit time is

$$\frac{dE}{dt} = (2\pi)^{-3} \int d^3k \sum_{\omega} \hbar\omega \; W(k\omega) \; . \tag{20}$$

The perturbation theory by which $W(k\omega)$ was derived must conserve energy and momentum (even though this was not explicitly indicated). Thus, if $\vec{P}_i$, $\vec{P}_f$ are the initial and final electron momentum for a given collision,

$$\vec{P}_i = \vec{P}_f + \hbar\vec{k} \; , \tag{21a}$$

$$\frac{1}{2M} P_i^2 = \frac{1}{2M} P_f^2 + \hbar\omega \tag{21b}$$

or

$$\hbar\omega = \frac{\hbar\vec{k} \cdot \vec{P}_i}{M} - \frac{(\hbar\vec{k})^2}{2M} \; . \tag{21c}$$

We assume $\hbar k \ll P_i$ (which may not be true when the electron energy is less than about 5 eV), so the last term in Eq. (21c) can be dropped. Thus, the sum over ω can be replaced by an integral times a delta function:

$$\frac{dE}{dt} = \frac{e^2}{\pi^2} \int d^3k \, k^{-2} \int d\omega \; \delta(\omega - k \cdot v) \; \mathrm{Im}\epsilon^{-1} \; . \tag{22}$$

We now use cylindrical coordinates for k, with the axis along v, and integrate over $dk_{\parallel}$ to remove the delta function. We also assume ϵ to be

independent of k. All of these steps reduce Eq. (22) to

$$\frac{dE}{dt} = \frac{2e^2}{v\pi} \int d\omega \, \mathrm{Im}\epsilon^{-1} \int \frac{k_\perp \, dk_\perp}{k^2 + (\omega/v)^2} \, . \tag{23}$$

The conservation of momentum has not been completely specified by just ensuring that Eq. (21c) is satisfied. If we look at the following scattering diagram

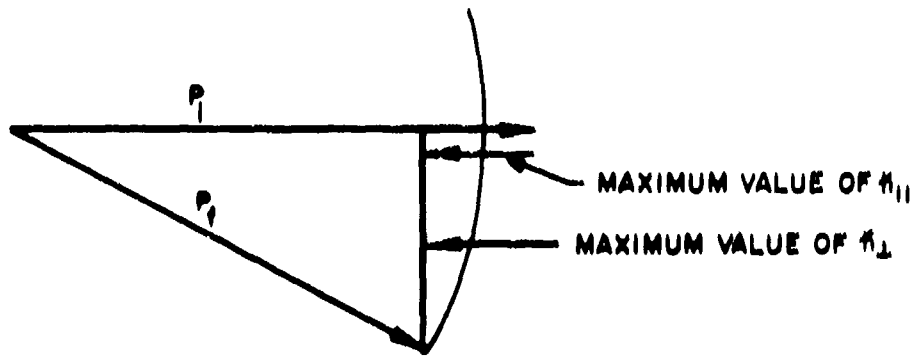

we see that requiring $\hbar k_{\|}$ to be small also forces $\hbar k_\perp$ to be small. Thus we take

$$k_\perp \lesssim \gamma\omega/v \, , \tag{24}$$

where γ is some number of order unity. The integral of Eq. (23) over $k_\perp$ will thus give a numerical factor of $1/2 \log (\gamma^2 + 1)$, which is henceforth dropped.

Finally, we remark that the electron can scarcely lose more energy in a collision than it has initially; i.e., there is an upper bound on ω. Equation (23) has now been reduced to the simple form

$$\frac{dE}{dt} = \frac{2e^2}{\pi v} \int_0^{E/\hbar} \omega \, d\omega \, \mathrm{Im}\epsilon^{-1} \, . \tag{25}$$

6.4 NUMERICAL ESTIMATES OF RANGE

The job now (apart from justifying a great number of assumptions!) is to evaluate the integral in Eq. (25) for materials of interest, which has not actually been done yet. It has, however, proven to be useful in evaluating the order of magnitude of dE/dt as it is determined by the various excitations that occur. As an example, suppose the dielectric constant is composed of the sum of three terms

$$\epsilon = 1 + \epsilon_d + \epsilon_{ph} + \epsilon_{ex} , \tag{26}$$

where

$$\epsilon_d = \frac{\epsilon_1}{1 - i\omega\tau_d} \qquad \text{dipole term,} \tag{27a}$$

$$\epsilon_{ph} = \frac{\epsilon_2}{1 - (\omega/\omega_p)^2 - i\omega\tau_p} \qquad \text{optical phonon,} \tag{27b}$$

$$\epsilon_{ex} = \frac{\epsilon_3}{1 - (\omega/\omega_{ex})^2 - i\omega\tau_{ex}} \qquad \text{exciton,} \tag{27c}$$

For completeness, a band-to-band term and a plasmon term should also be included for the energy losses below 5 to 25 eV,[12] but more time would be required to include them.

The resonance contributions, ϵ_{ph} and ϵ_{ex}, have a rapid variation only in the region of their resonant frequency. We can therefore make the approximation

$$\epsilon \approx \bar{\epsilon}_d + \frac{\epsilon_1(1 + i\omega\tau_d)}{1 + (\omega\tau_d)^2} \qquad 0 \le \omega \lesssim \omega_{ph} , \tag{28a}$$

$$\approx \bar{\epsilon}_{ph} + \frac{\epsilon_2 [1 - (\omega/\omega_p)^2 + i\omega\tau_{ph}]}{[1 - (\omega/\omega_{ph})^2]^2 + [\omega\tau_{ph}]^2} \qquad \omega_{ph} \le \omega \le \omega_{ex} , \tag{28b}$$

$$\approx 1 + \frac{\epsilon_3 \left[1 - (\omega/\omega_{ex})^2 + i\omega\tau_{ex}\right]}{\left[1 - (\omega/\omega_{ex})^2 + [\omega\tau_{ex}]^2\right]} \qquad \omega_{ex} \lesssim \omega . \tag{28c}$$

In Eqs. (28a) and (28b),

$$\overline{\epsilon_d} = 1 + \epsilon_2 + \epsilon_3 , \tag{29a}$$

$$\overline{\epsilon_{ph}} = 1 + \epsilon_3 . \tag{29b}$$

At this stage we are interested in a rough answer (the input ϵ is only a guess based on a plausible model), so we shall estimate the integrals in a crude manner. For $\omega \lesssim \omega_{ph}$,

$$\omega \mathrm{Im}\,\epsilon^{-1} \alpha \frac{\epsilon_1 \omega\,(1 + \omega\tau_d)}{1 + (\omega\tau_d)^2} \to \epsilon_1/\tau_d \quad \text{for } \omega \gg \tau_d^{-1} . \tag{30}$$

We assume $\tau_d^{-1} \ll \omega_{ph}$, so the large constant region of the integrand will dominate the integral.

The integrand in the region of a resonance is

$$\omega \mathrm{Im}\,\epsilon^{-1} \approx \frac{\epsilon\,\omega\omega\tau}{[1 - (\omega/\omega_0)^2]^2 + (\omega\tau)^2} . \tag{31}$$

This is a peak with a height of $1/\tau$ and a width of about $\omega_0^2\tau$. Thus, these integrals are independent of the damping and depend only on the energy of the resonance.

We can now collect the above estimate to find the energy loss per unit distance, as given by Eq. (25), to be

$$dE/dx = (a_0 \pi E)^{-1} \begin{cases} \dfrac{\epsilon_1 \hbar E}{(\bar{\epsilon}_d)^2 \tau_d} & E \leq \hbar\omega_{ph} , \\ \dfrac{\epsilon_1 \hbar^2 \omega_{ph}}{(\bar{\epsilon}_d)^2 \tau_d} + \dfrac{\epsilon_2 (\hbar\omega_{ph})^2}{\bar{\epsilon}_2^2} & h\omega_{ph} \leq E \leq \hbar\omega_{ex} , \\ \dfrac{\epsilon_1 \hbar^2 \omega_{ph}}{(\bar{\epsilon}_d)^2 \tau_d} + \dfrac{\epsilon_2 (\hbar\omega_{ph})^2}{\bar{\epsilon}_2^2} + \epsilon_3 (\hbar\omega_{ex})^2 & E \geq h\omega_{ex} . \end{cases} \quad (32)$$

In Eq. (32), a_0 is the Bohr radius.

The various energies are far enough removed that the highest term appearing in Eq. (32) will dominate. This being the case, we can make the simple physical interpretation that the range for the various processes will just add. That is, there will be a certain range, R_{ex}, while the electron is losing energy down to E_{ex}, another range while it loses energy down to E_{ph}, etc. Thus,

$$R = R_d + R_{ph} + R_{ex} \quad (33)$$

with

$$R_{ex} \approx (a_0 \pi \epsilon_3)^{-1} [(E_0^2/E_{ex})^2 - 1] , \quad (34a)$$

$$R_{ph} \approx (a_0 \pi \epsilon_2)^{-1} \bar{\epsilon}_{ph}^2 [(E_{ex}/E_{ph})^2 - 1] , \quad (34b)$$

$$R_d \approx (a_0 \pi \epsilon_1) \bar{\epsilon}_d^2 [\omega_{ph} \tau_d - (\tau_d E_0/\hbar)] . \quad (34c)$$

For example, suppose an insulator has an exciton band at 3 eV, optical modes at 3×10^{-2} eV, and dipolar relaxation times below 10^{10} Hz ($\hbar/\tau_d \approx 10^{-5}$ eV), and we inquire into the range of a 15-eV electron. From Eq. (34a), this electron will travel about 25 Å while losing energy down to 3 eV; it will then travel of the order of 10^4 Å (assuming $\bar{\epsilon}_{ph} \approx 1$, the range will be 10^5 if $\bar{\epsilon}_{ph}$ is as large as 3) while slowing down to 3×10^{-2} eV; and, finally, it will travel about 3×10^5 Å as it slows down

to, say, 3×10^{-3} eV. (This last range assumes $\epsilon_1 \approx 10^{-2}$; as it should be if the material is a good dielectric.)

As a final estimate, the energy loss to acoustic phonons is examined, which, again, is done with the aid of a simple model rather than relying too strongly on first principles. The last term in Eq. (18), which gives the energy lost to acoustic phonons, involves exactly the same matrix elements that are needed to find the relaxation time that determines the mobility. (Already another simplification has been made. It is assumed the electrons do not couple to the optical modes so well that they are accompanied by a virtual polarization cloud; i.e., the material could be silicon or probably Mylar, but not magnesium oxide.)

These matrix elements do not depend on the energy of the electron.[2] The energy loss per unit time given by Eq. (20) is thus approximately equal to

$$\frac{dE}{dt} = (2\pi)^{-3} W \sum_{\omega} \hbar\omega \Delta(\omega) , \tag{35}$$

where $\Delta(\omega)$ is the volume of k space allowed in the scattering event that creates a phonon of energy $\hbar\omega$ and $W(k,\omega)$ has been set equal to the constant W.

A diagram of the initial and final momentum is shown in Fig. 6.1. The energy and momentum conservation rules that must accompany Fig. 6.1 are, for small ΔP,

$$\frac{\Delta P \cdot P_i}{M} \approx \hbar\omega \tag{36}$$

and

$$\Delta \vec{P} = \hbar(\vec{k} + \vec{g}) , \tag{37}$$

where $\vec{g}$ is a reciprocal lattice vector. This vector must be added to $\vec{k}$ to include Umklapp processes which can occur in solids. Since energies as low as 5 eV are of concern here, the occurrence of such processes is important since only if Umklapp scatterings occur can the entire circle shown in Fig. 6.1 be reached by $\vec{P}_f$.

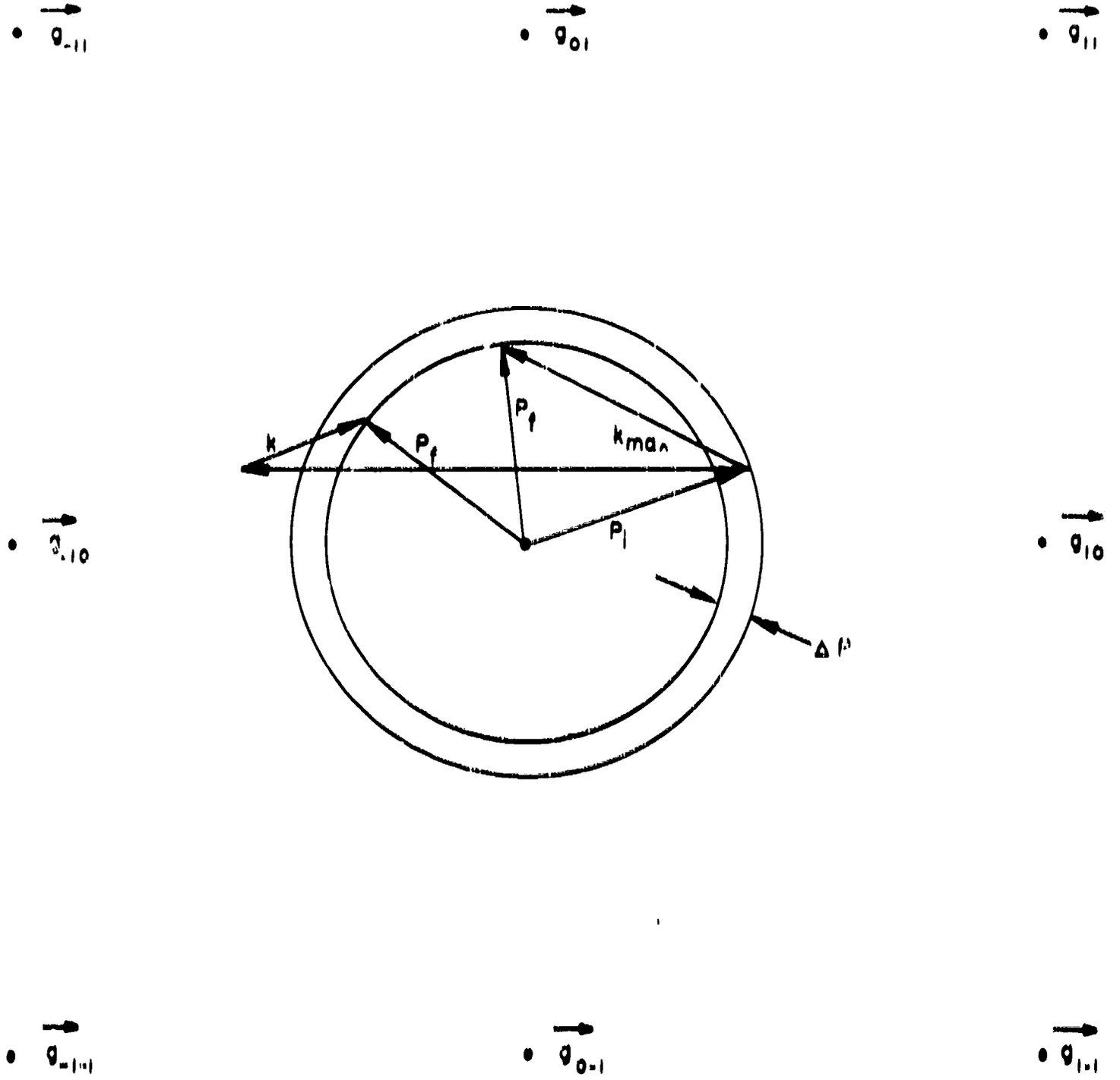

Fig. 6.1--Diagram showing two scattering events that lead to the same value of $|P_f|$. Since $|k| = |k_{max}|$, the larger-angle scattering would be forbidden without Umklapp processes. ΔP, greatly exaggerated in the drawing, is at most a few percent of P

The actual value of $\Delta(k)$ will be rather complicated, but the order of magnitude is clearly seen to be

$$\Delta(k) \approx 4\pi P(\Delta P \cdot P_i) \approx 4\pi MP\hbar\omega \ . \tag{38}$$

Thus,

$$\frac{dE}{dt} \approx (2\pi^2)^{-2} \ WPM \sum_{\omega} (\hbar\omega)^2$$

$$\approx (2\pi^2)^{-2} \ WPM \ (k\theta)^2 \ . \tag{39}$$

In Eq. (39), the sum over the phonon energies has been replaced by the average phonon energy. This quantity, in turn, has been replaced by the Debye temperature θ.

From Eq. (39), the energy loss per unit distance is a constant, independent of the electron energy. This can be interpreted in terms of a very simple model; namely, that the electron has a constant mean free path, λ, with

$$\lambda = 2\pi^2 \ [M^2(k\theta)W]^{-1} \ , \tag{40}$$

and that at each scattering it loses an amount of energy $k\theta$.

The numerical value of λ can be estimated from the mobility μ. For a good insulator, a mobility of about 30 $cm^2/sec \ V$ is assumed. This corresponds to a relaxation time of

$$\tau = m\mu/e$$

$$\tau \approx \frac{9 \times 10^{-28} \times 30 \ cm^2}{sec \ eV} \approx \frac{2.7}{1.6} \times 10^{-14} \ sec \ . \tag{41}$$

The velocity of an electron with energy kT is a little more than 10^7 $cm \ sec^{-1}$, so

$$\lambda \approx 2 \times 10^{-7} \ cm \ , \tag{42}$$

The linear range is

$$R = \int \frac{dE}{dE/dx} = \frac{\lambda}{k\theta} (E_0 - E_f) \ . \tag{43}$$

If $E_0 \approx 3$ eV and $E_f \approx 0.03$ eV, then

$$R \approx 2 \times 10^4, \tag{44}$$

which is about the same as that found for optical phonons.

The linear range, of course, greatly overestimates the total projected range, $|\vec{R}|$, traversed by the electron. Fortunately, this projected range can be easily estimated for energy loss to phonons. According to the model already mentioned, the electron loses the same amount of energy, $k\theta$, which is typically 0.03 eV, at each collision, and thus it must suffer N collisions, where

$$N = E_0/k\theta \tag{45}$$

is about 100 for an E_0 of 3 eV. From standard random-walk theory, one knows that the projected range is simply

$$|\vec{R}| \approx \lambda \sqrt{N} \approx 2 \times 10^3 \text{ Å}. \tag{46}$$

Since the loss to optical phonons is about the same, but perhaps somewhat larger, the projected range due to both processes will be about one-half of the value given in Eq. (46).

6.5 CONCLUSIONS

It should be remembered that only a rough estimate of the range has been made here. Even if the approximations made in the derivations of the final formulas are valid, the material parameters used to find numerical values are only a guess based on typical values encountered for well-studied materials. Numbers specific to a practical insulator such as Mylar are not known.

If these numbers do not prove to be too wide of the mark, however, then it is found that the electron will slow down very rapidly (a linear range of 25 Å) from 15 eV to 3 eV as it loses energy to excitons, and then it will lose energy about equally to optical and acoustical phonons. The projected range is estimated to be about 10^3 Å as the electron slows down from 3 eV to thermal energies.

7. CONCLUSIONS

The ion implantation process has been successfully utilized to apply metallic contacts to semiconductors and insulators. The transient response of a Mylar capacitor with ion-implanted contacts displayed reduced polarization effects but no significant decrease in response which would make its use desirable in radiation environments. The ion-implanted electrodes exhibited better carrier injection than foil electrodes and allowed ohmic contacts to be applied to semiconductors with a wide range of resistivity; consequently, the process has advantages in research work where simpler methods fail to provide good contacts. The production use of the process for capacitors is doubtful owing to the lengthy cleaning procedure and the difficulty of achieving a uniform plasma with the associated equipment necessary for implantation on a continuous film.

The transient radiation response exhibited by a Mylar capacitor versus temperature is consistent with the response predicted by a band model of the conduction process in which traps are uniformly distributed in the forbidden zone and one sign of carrier is immobilized. Under such conditions, the photocurrent is extremely small compared to that displayed without trapping and a weak dependence of the photocurrent on temperature is predicted. The observed decay time constant can be many orders of magnitude longer than the average carrier lifetime and is insensitive to temperature.

New methods of fabricating ceramic and glass capacitors with high dielectric constants have yielded large capacity-to-volume ratios and consequently the prompt radiation response is small. The use of these capacitors is still limited, however, since the temperature coefficients of capacity are large, and this prevents the use of such capacitors in critical circuit applications where the capacity must remain constant for proper circuit functions over a large temperature range.

Examination of the energy loss of moderately fast electrons in insulators, which is necessary for the theory of transient radiation effects in insulators,[1] indicates that energy loss to excitons is the primary process that occurs in the energy range from 15 eV to 3 eV. Energy loss to optical and acoustical phonons then occurs down to thermal energies.

Previous work under this contract has shown that anomalously large transient effects measured in small-valued mica capacitors could be

ascribed to leakage currents through air trapped inside the capacitor encapsulation.[4] Comparison of the transient response of a commercial mica capacitor with that of a similar capacitor that had a conductive coating on the encapsulation demonstrated that electric charge from ionized air can be trapped on the insulator surface, leading to increased initial transient signals.[23] Irradiation of several capacitors using different dielectric materials in a TRIGA reactor indicated that neutron response was least sensitive in ceramic capacitors followed by mica, tantalum oxide, and Mylar dielectrics.[23] A method for verification of a model for neutron irradiation of dielectrics by proton irradiation was described.[4] A capacitor exchange program in which the same capacitors were measured by General Atomic and International Business Machines indicated that measurements performed with an RC circuit in which charge transfer was measured yielded comparable results to measurement of radiation-induced current with current probes.[23]

REFERENCES

1. DeMichele, D. W., D. K. Nichols, and V. A. J. van Lint, Radiation Effects on Dielectric Materials, Quarterly Report No. 3, U. S. Army Electronics Command, Technical Report ECOM-01412-3, July 1966.

2. Overmyer, R. F., Radiation Effects on Dielectric Materials, Quarterly Report No. 4, U. S. Army Electronics Command, Technical Report ECOM-01412-4, October 1966.

3. van Lint, V. A. J., B. E. Kott, and D. E. Willis, Transient Radiation Effects on Electronic Parts, Report No. 8, Eighth Quarterly Progress Report, Contract DA36-039SC-89196, General Atomic Division, General Dynamics Corporation, Report GA-5211, June 1964.

4. Overmyer, R. F., D. K. Nichols, and V. A. J. van Lint, Radiation Effects on Dielectric Materials, Quarterly Report No. 1, U. S. Army Electronics Command, Technical Report ECOM-01412-1, December 1965.

5. Mattox, D. M., "Film Deposition Using Accelerated Ions," Sandia Corporation, Reprint SC-R-64-1344, November 1964.

6. _____, "Metallizing Ceramics Using a Gas Discharge," Sandia Corporation, Reprint SC-R-64-1330, September 1964.

7. _____, "Interface Formation and the Adhesion of Deposited Thin Films," Sandia Corporation, Monograph SC-R-65-852, January 1965.

8. _____, "Design Considerations for Ion Plating," Sandia Corporation, Reprint SC-R-65-997, January 1966.

9. Rose, A., RCA Review, Vol. 12, No. 3, 1951, p. 362.

10. van Lint, V. A. J., E. G. Wikner, R. Denson, H. Horiye, H. K. Lintz, D. K. Nichols, and R. A. Poll, Transient Radiation Effects, Final Report, Contract DA-49-186-AMC-65(X), General Atomic Division, General Dynamics Corporation, Report GA-6248, March 22, 1965.

11. van Lint, V. A. J., R. F. Overmyer, and D. K. Nichols, Transient Radiation Effects on Electronic Parts, Final Report, Contract DA36-039SC-89196, General Atomic Division, General Dynamics Corporation, Report GA-6534, July 10, 1965.

12. Sternheimer, R. M., in Methods of Experimental Physics, Vol. 5, Part A, Chien-Shiung Wu and E. C. L. Wuan, eds., Academic Press, New York, 1961, pp. 1-76.

13. Fröhlich, H., and H. Pelzer, Proc. Phys. Soc. (London), Vol. A68, 1955, p. 525.

14. _____, and R. L. Platzman, "Energy Loss of Moving Electrons to Dipolar Relaxation," Phys. Rev., Vol. 92, 1953, p. 1152.

15. Pines, D., Elementary Excitations in Solids, W. A. Benjamin, Inc., New York, 1963, pp. 123 ff.

16. Debye, P., Polar Molecules, Dover Publications, 1929, Sec. 29.

17. Kittel, C., Introduction to Solid State Physics, 2d ed., John Wiley & Sons, Inc., New York, 1953.

18. Ziman, J. M., Electrons and Phonons, Clarendon Press, Oxford, 1960, Secs. 5, 6, 5, 9.

19. _____, Principles of the Theory of Solids, Cambridge University Press, Vol. II, 1964, Sec. 6, 13.

20. Feynman, R. P., et al., The Feynman Lectures on Physics, Vol. II, Addison-Wesley Press, 1964, Sec. 10, 4.

21. Nichols, D. K., and V. A. J. van Lint, Solid State Physics, Vol. 18, 1966, p. 22.

22. Compton, D. M. J., private communication.

23. Overmyer, R. F., D. K. Nichols, and V. A. J. van Lint, Radiation Effects on Dielectric Materials, Quarterly Report No. 2, U. S. Army Electronics Command, Technical Report ECOM-01412-2, March 1966.

(security classification of title, body of abstract and indexing annotation must be entered when the overall report is classified)

1. ORIGINATING ACTIVITY (Corporate author)	2a. REPORT SECURITY CLASSIFICATION
General Atomic Division General Dynamics Corporation San Diego, California	Unclassified 2b GROUP

3. REPORT TITLE

RADIATION EFFECTS ON DIELECTRIC MATERIALS

4. DESCRIPTIVE NOTES (Type of report and inclusive dates)

Final Report (1 July 1966 through 30 September 1966)

5. AUTHOR(S) (Last name, first name, initial)

J. F. Colwell, D. W. De Michele, R. F. Overmyer

6. REPORT DATE	7a. TOTAL NO OF PAGES	7b. NO. OF REFS
December 1966	56	23

8a. CONTRACT OR GRANT NO.	9a. ORIGINATOR'S REPORT NUMBER(S)
DA28-043AMC-01412(E) b AMC Code 5900.21.830.4400 c d	GA-7474 9b. OTHER REPORT NO(S) (Any other numbers that may be assigned this report) ECOM-01412-F

10. AVAILABILITY/LIMITATION NOTICES

Distribution of this document is unlimited

11. SUPPLEMENTARY NOTES	12. SPONSORING MILITARY ACTIVITY
This research was sponsored by the Defense Atomic Support Agency under NWER Subtask 16.0091	U.S. Army Electronics Command Fort Monmouth, N. J. 07703 AMSEL-KL-U3

13 ABSTRACT

A detailed description of the techniques and equipment employed in the ion-implantation process is presented. Results of high-energy electron irradiation of a Mylar capacitor with ion-implanted electrodes are compared to the response of a control sample. The ion-implanted electrodes exhibit better carrier injection than conventional foil electrodes. Transient radiation effects data from irradiation of a monolithic ceramic capacitor and two glass capacitors are included. One of the glass capacitors contained a semicrystalline dielectric with very high dielectric constant. The transient radiation effects in Mylar versus temperature appear to fit a band model for the conduction process in which a continuous distribution of carrier traps is located in the forbidden zone and one sign of carrier is immobilized. An examination of the energy loss processes of moderately fast electrons in insulators indicates that from 15 eV to 3 eV the energy loss is primarily to excitons whereas energy loss to optical and acoustical phonons occurs down to thermal energies.

DD FORM 1 JAN 64 1473

Security Classification

14 KEY WORDS	LINK A		LINK B		LINK C	
	ROLE	WT	ROLE	WT	ROLE	WT
Radiation-induced conductivity						
Radiation effects in dielectrics						
Radiation effects in capacitors						
Transient radiation effects						
Ion plating						
Ion implantation						
Electron energy loss						

INSTRUCTIONS

1. ORIGINATING ACTIVITY: Enter the name and address of the contractor, subcontractor, grantee, Department of Defense activity or other organization *(corporate author)* issuing the report.

2a. REPORT SECURITY CLASSIFICATION: Enter the overall security classification of the report. Indicate whether "Restricted Data" is included. Marking is to be in accordance with appropriate security regulations.

2b. GROUP: Automatic downgrading is specified in DoD Directive 5200.10 and Armed Forces Industrial Manual. Enter the group number. Also, when applicable, show that optional markings have been used for Group 3 and Group 4 as authorized.

3. REPORT TITLE: Enter the complete report title in all capital letters. Titles in all cases should be unclassified. If a meaningful title cannot be selected without classification, show title classification in all capitals in parenthesis immediately following the title.

4. DESCRIPTIVE NOTES: If appropriate, enter the type of report, e.g., interim, progress, summary, annual, or final. Give the inclusive dates when a specific reporting period is covered.

5. AUTHOR(S): Enter the name(s) of author(s) as shown on or in the report. Enter last name, first name, middle initial. If military, show rank and branch of service. The name of the principal author is an absolute minimum requirement.

6. REPORT DATE: Enter the date of the report as day, month, year; or month, year. If more than one date appears on the report, use date of publication.

7a. TOTAL NUMBER OF PAGES: The total page count should follow normal pagination procedures, i.e., enter the number of pages containing information.

7b. NUMBER OF REFERENCES: Enter the total number of references cited in the report.

8a. CONTRACT OR GRANT NUMBER: If appropriate, enter the applicable number of the contract or grant under which the report was written.

8b, 8c, & 8d. PROJECT NUMBER: Enter the appropriate military department identification, such as project number, subproject number, system numbers, task number, etc.

9a. ORIGINATOR'S REPORT NUMBER(S): Enter the official report number by which the document will be identified and controlled by the originating activity. This number must be unique to this report.

9b. OTHER REPORT NUMBER(S): If the report has been assigned any other report numbers *(either by the originator or by the sponsor)*, also enter this number(s).

10. AVAILABILITY/LIMITATION NOTICES: Enter any limitations on further dissemination of the report, other than those imposed by security classification, using standard statements such as:

(1) "Qualified requesters may obtain copies of this report from DDC."

(2) "Foreign announcement and dissemination of this report by DDC is not authorized."

(3) "U. S. Government agencies may obtain copies of this report directly from DDC. Other qualified DDC users shall request through _____."

(4) "U. S. military agencies may obtain copies of this report directly from DDC. Other qualified users shall request through _____."

(5) "All distribution of this report is controlled. Qualified DDC users shall request through _____."

If the report has been furnished to the Office of Technical Services, Department of Commerce, for sale to the public, indicate this fact and enter the price, if known.

11. SUPPLEMENTARY NOTES: Use for additional explanatory notes.

12. SPONSORING MILITARY ACTIVITY: Enter the name of the departmental project office or laboratory sponsoring *(paying for)* the research and development. Include address.

13. ABSTRACT: Enter an abstract giving a brief and factual summary of the document indicative of the report, even though it may also appear elsewhere in the body of the technical report. If additional space is required, a continuation sheet shall be attached.

It is highly desirable that the abstract of classified reports be unclassified. Each paragraph of the abstract shall end with an indication of the military security classification of the information in the paragraph, represented as (TS), (S), (C), or (U).

There is no limitation on the length of the abstract. However, the suggested length is from 150 to 225 words.

14. KEY WORDS: Key words are technically meaningful terms or short phrases that characterize a report and may be used as index entries for cataloging the report. Key words must be selected so that no security classification is required. Identifiers, such as equipment model designation, trade name, military project code name, geographic location, may be used as key words but will be followed by an indication of technical context. The assignment of links, rules, and weights is optional.

DD FORM 1473